Applied Catalysis B: Environmental 328 (2023) 122524

Contents lists available at ScienceDirect

Applied Catalysis B: Environmental

journal homepage: www.elsevier.com/locate/apcatb

A redox model for NO oxidation, NH_3 oxidation and high temperature standard SCR over Cu-SSZ-13

Rohil Daya [a,*], Dhruba J. Deka [b], Anshuman Goswami [c], Unmesh Menon [a], Dylan Trandal [a], William P. Partridge [b], Saurabh Y. Joshi [a]

[a] Cummins Inc., 1900 McKinley Ave, Columbus, IN 47201, United States
[b] Oak Ridge National Laboratory, 2360 Cherahala Blvd., Knoxville, TN 37932, United States
[c] University of Notre Dame, Notre Dame, IN 46556, United States

ARTICLE INFO

Keywords:
Selective catalytic reduction
Kinetic model
Hydrothermal aging
Cu-zeolites
Brønsted acid sites

ABSTRACT

A kinetic model is developed to predict the influence of temperature and hydrothermal aging on the redox of active Cu sites under standard SCR, NO oxidation and NH_3 oxidation conditions over a practically relevant fully-formulated Cu-SSZ-13 catalyst. NO_2/N_2 production during NO/NH_3 titration of Cu^{II} sites is utilized to identify rate parameters associated with NO-only RHC (reduction half cycle) and NH_3-only RHC respectively. Integral N_2 formation during subsequent NO + NH_3 titration is consistent with the production of one NO_2 per two Cu^{II} sites reduced during NO-only RHC and one N_2 per six Cu^{II} sites reduced during NH_3-only RHC. Decreased reduction of Cu^{II} sites by NO/NH_3 upon hydrothermal aging, along with the production of one NO_2 per two Cu^{II} sites during NO-only RHC, is accordant with the involvement of proximal ZCuOH and oxygen-bridged dimeric Cu^{II} sites. Oxidation of partially solvated and framework coordinated ZCu (Cu^{I}) sites occurs in presence of O_2, does not produce N_2 and can lead to the consumption of Brønsted acid sites. A global OHC kinetic model is developed to predict transient and integral N_2 formation during exposure of Cu^{I} sites to a mixture of NO and O_2. The resulting redox kinetic model quantitatively predicts NO and NH_3 consumption during isothermal transient response Cu redox (TRCR) protocols, along with temperature and age dependent steady-state standard SCR and oxidation conditions. The redox model presented in this work synthesizes recent kinetic, spectroscopic and computational findings to provide a foundational description of active site redox during standard SCR, NO oxidation and NH_3 oxidation over Cu-SSZ-13.

1. Introduction

Small pore SSZ-13 zeolites exchanged with Copper (Cu) ions are utilized for the selective catalytic reduction (SCR) of nitrogen oxides (NO_x) produced in lean-burn engines to N_2 [1,2]. The configuration of ion-exchanged active Cu sites is influenced by the distribution of framework aluminum (Al_f) in the zeolite, which in turn depends on composition parameters (such as Si/Al ratio) and synthesis methods [3–8]. Experimental and theoretical studies have established energetically stable and chemically distinct configurations of monomeric Cu associated with paired Al_f in the double six-membered ring (labeled Z_2Cu), and with isolated Al_f in the eight-membered ring (8MR) chabazite cage (labeled ZCuOH) [3,6,7,9]. In addition, stable dimeric Cu configurations associated with paired Al_f in the 8MR (or 8MR-6MR combinations) have been identified (such as Z_2Cu_2O, $Z_2Cu_2O_2H_2$ etc.) [10–15].

Standard SCR proceeds via a redox mechanism involving transformations between monomeric and dimeric Cu configurations [16–22]. The initial configuration of Cu ions is dependent on the temperature, O_2 pressure and H_2O pressure [13,15]. Presence of excess H_2O below 250 °C leads to the formation of hydrated Cu complexes detached from the zeolite framework [3]. Introduction of NH_3 leads to preferential binding relative to H_2O, and formation of mobile Cu-amine complexes [3,23,24]. These complexes are subsequently reduced in presence of NO, and re-oxidized in presence of O_2. Pioneering work on the low-temperature SCR mechanism has led to the understanding that both the reduction half cycle (RHC) and the oxidation half cycle (OHC) involve the formation of multinuclear sites from pairs of Cu-amine complexes [16,17,20,25]. However, the correlation between the Cu^{II}-dimeric complex expected to form during RHC ($Z_2Cu_2O_2H_2(NH_3)_2$) and during OHC ($Z_2Cu_2O_2(NH_3)_4$) remains unclear. This understanding is

* Corresponding author.
E-mail address: rohil.daya@cummins.com (R. Daya).

https://doi.org/10.1016/j.apcatb.2023.122524
Received 22 November 2022; Received in revised form 18 January 2023; Accepted 23 February 2023
Available online 24 February 2023

necessary to close the overall standard SCR redox cycle and explain the measured integral NO consumption during sequential isothermal Cu redox experiments [21,26,27].

Increasing temperatures leads to NH_3 de-solvation and framework coordination of Cu ions, postulated as the origin of the decrease in NO_x conversion near 350 °C [2,17,28]. At high temperatures, framework coordinated Cu^{II} ions are completely reduced in presence of NO and NH_3 [21,27]. Oxidation of the resulting framework coordinated Cu^{I} ions under SCR conditions is proposed to proceed via multiple pathways, including formation of Cu-nitrate intermediates and consumption of Brønsted NH_3 [7,29,30]. Spectroscopic and transient response kinetic experiments have demonstrated that the reduction half cycle (RHC) is SCR rate limiting at high temperatures [27,31]. Under these conditions, competing NO and NH_3 oxidation reactions also occur [2]. NO oxidation is proposed to follow a redox mechanism over oxygen-bridged dimeric Cu configurations, involving nitrite, nitrate and/or nitrosonium ion intermediates [32–35].

Exposure of the catalyst to NH_3 in absence of O_2 leads to reduction of Cu^{II} ions to Cu^{I} [36–39]. The onset temperature of reduction is ~200 °C in absence of H_2O, and increases to ~300 °C in presence of H_2O [37,38]. The mechanism associated with the NH_3-only RHC is not well understood. Gao et al. [33] proposed the formation of Cu^{II} dimers upon NH_3 solvation below 350 °C, consistent with the reported second order dependence of NH_3 oxidation rates on Cu loading. This hypothesis is also consistent with the recent finding on the low temperature NO + NH_3 titration of Cu^{II} ions involving NH_3-solvated Cu^{II} dimers [25]. At temperatures above 350 °C, reduction of Cu^{II} ions in presence of NH_3 may proceed via dissociation of NH_3 across the Cu-O framework, leading to NH_2 formation [31,40,41]. The stoichiometry of the NH_3-only RHC is reported to be one N_2 produced per Cu^{II} reduced using NH_3 temperature programmed reduction (TPR) methods [42], and one N_2 produced per six Cu^{II} reduced from NH_3 temperature programmed desorption (TPD) and isothermal NH_3 titration [38,43,44]. Wilcox et al. [44] rationalized the $6Cu^{II}$:1 N_2 stoichiometry by invoking mobile Cu-amine complexes and reactive intermediates such as H_2. Under dry conditions, complete reduction of Cu^{II} to Cu^{I} by NH_3 is observed [43,44]. However, experiments in presence of H_2O suggest the exclusive involvement of nominally ZCuOH sites [38], consistent with the observed decrease in NH_3 oxidation rates upon hydrothermal aging [45].

The direct oxidation of framework coordinated Cu^{I} ions to Cu^{II} (in presence of O_2) is necessary to close the NO oxidation redox cycle, and the high temperature NH_3 oxidation redox cycle. This direct oxidation reaction has been investigated in the partial methane oxidation (PMO) literature, and is proposed to involve the formation of mono (μ-oxo) dicopper (II) species (Z_2Cu_2O) from pairs of framework coordinated Cu^{I} ions [46–49].

A self-consistent and experimentally validated kinetic model describing active Cu redox during high temperature standard SCR, NO oxidation and NH_3 oxidation over Cu-zeolites has not been previously reported in literature. Recently, we proposed a kinetic model to describe the redox of active Cu sites under low temperature standard SCR conditions, along with the reduction of framework coordinated Cu^{II} ions by NO and NH_3 [21]. In the present work, this redox model framework is extended to include the reduction of Cu^{II} ions to Cu^{I} in presence of NO or NH_3, along with the re-oxidation of partially-solvated (by NH_3) and framework coordinated Cu^{I} ions in presence of O_2. Section 2 details the transient kinetic experiments utilized for identifying and validating rate parameters in the redox model. In Section 3.1, NO titration experiments are utilized to develop the kinetics associated with the reversible reduction of Cu^{II} ions in presence of NO. Similarly, Section 3.2 utilizes NH_3 titration experiments to identify rate parameters associated with the reduction of Cu^{II} ions in presence of NH_3. Oxidation of partially solvated and framework coordinated Cu^{I} ions results in the formation of dimeric Cu^{II} configurations, which can transform to monomeric ZCuOH sites that are subsequently reduced by NO. Global OHC kinetics are developed in Section 3.3 to predict transient and integral N_2 formation during exposure of Cu^{I} ions to a mixture of NO and O_2. NH_3 TPD experiments after isothermal reduction-oxidation of an NH_3-saturated catalyst in alternating feeds of NO and O_2 are described in Section 3.4, highlighting a pathway for the transfer of Brønsted NH_3 to Lewis NH_3. The resulting redox model is validated using transient response Cu-redox (TRCR) protocols in section 3.5. Implications of the model on the redox mechanism relevant for standard SCR, NO oxidation and NH_3 oxidation reactions are discussed in Section 4.

The redox model presented here utilizes spectroscopic and transient kinetic experiments to predict operando changes in configurations, oxidation state and surface coverages of active Cu sites, relating these changes in the material surface with the measured conversions of gas species under SCR and oxidation conditions.

2. Transient kinetic experiments

2.1. Micro core experiments with SpaciMS

Bench-flow reactor data on a state-of-the art Cu-SSZ-13 catalyst (Cu loading ~2.4 wt% and Si/Al ~15) was utilized for developing the redox kinetic model. All details regarding experimental setup can be found in reference [27]. A 0.3″ diameter and 1″ long micro core was extracted from the full-scale cordierite monolith (600 cells per square inch, 0.003″ wall thickness) washcoated with a fully-formulated Cu-SSZ-13 catalyst. Prior to RHC and OHC experiments, the catalyst was degreened at 550 °C for 4 h in a base feed containing 10% O_2, 7% H_2O, 8% CO_2 and balance Ar. The catalyst was then cooled to a temperature between 200 °C and 450 °C, and the temperature was held constant during the experiment. Identical experiments were also conducted on a catalyst hydrothermally aged at 650 °C for 60 h in the same base feed. Prior to each run, the catalyst was oxidized in 5% O_2 at 450 °C.

A micro-reactor equipped with spatially resolved capillary inlet mass spectrometer (SpaciMS) was used to run the transient response Cu-redox cycle (TRCR) protocol (Fig. 1). In this protocol, 5% O_2, 200 ppm NH_3 and 200 ppm NO were switched in and out of the feed gas to perform transient standard SCR reaction (NO + NH_3 + O_2), RHC (NO + NH_3), and OHC (NO + O_2 or O_2-only); a constant 5% H_2O flow in balance Argon exists throughout the protocol. SpaciMS allows for measurements of gaseous species at multiple intra-catalyst locations, providing a spatially resolved map of transient reactant and product species, including N_2. Sampling from different intra-catalyst axial locations (from z/L = 1/16 to z/L = 1 where L represents the length of the catalyst) allowed measurements at gas hourly space velocity (GHSV) values between 40,000–640,000 h^{-1}, corresponding to a volumetric flow rate of ~0.82 SLPM (standard liters per minute). Detailed description of the 10-step TRCR protocol, along with interpretation of the experimental data on a degreened catalyst can be found in reference [27].

Reduction rates of Cu^{II} sites in presence of NO (without NH_3) were estimated through monitoring NO_2 formation using an FTIR in dedicated NO-only RHC experiments, described further in [38].

Minor NO/NH_3 consumption along with N_2 formation was observed

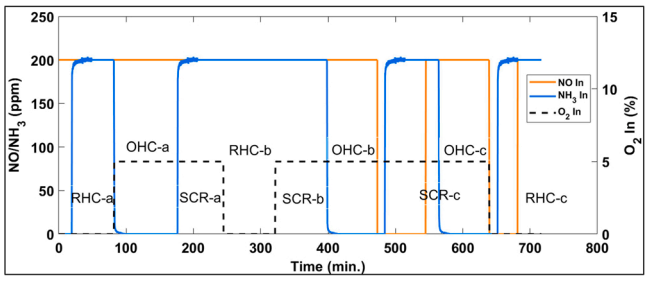

Fig. 1. Isothermal ten-step transient response Cu-redox (TRCR) experimental protocol.

at steady-state during RHC steps in the TRCR protocol, attributed to the presence of approximately 2 ppm contaminant O_2 in the reactor feed gases. Residual or contaminant O_2 originates from the gas standards, but most likely the Argon balance which is provided by a liquid-Argon dewar for the current work. High purity levels ~99.999% can also lead to noticeable steady-state SCR from ppm level O_2.

2.2. Pilot core experiments

Additional bench-flow pilot-reactor data on a different sample of the same Cu-SSZ-13 catalyst mentioned in Section 2.1 was utilized for developing and validating the redox kinetic model. All details regarding experimental setup can be found in [50]. A 1″ diameter and 3″ long pilot core was extracted from the full-scale monolith washcoated with a Cu-SSZ-13 catalyst. Prior to the RHC, OHC and SCR experiments, the catalyst was aged at the desired temperature and time in a base feed containing 10% O_2, 10% H_2O and balance N_2. This catalyst was then cooled to 200 °C and solvated in 200 ppm NH_3 in the presence of 8% CO_2, 7% H_2O, 10% O_2 (to minimize reduction of Cu^{II} sites) and balance N_2. The NH_3 TPD experiment was performed by ramping from 200 °C to 550 °C (with no isothermal desorption), under a gas mixture of 8% CO_2, 7% H_2O and balance N_2, at a rate of 10 °C/min. The consumption of Lewis NH_3 and Brønsted NH_3 during Cu-site redox was quantified through various reductive and oxidative treatments on the NH_3-saturated catalyst prior to the NH_3-TPD experiment. These variations included:

- Reduction by 200 ppm NO for 2 h
- One cycle of reduction by 200 ppm NO for 2 h followed by oxidation in 10% O_2 for 2 h
- Three cycles of reduction by 200 ppm NO for 2 h followed by oxidation in 10% O_2 for 2 h

Fig. 2a plots the NH_3 TPD experimental protocol for the variation with three redox cycles prior to TPD. Similar experimental protocols have been utilized previously by Usberti et al. [26] and Deka et al. [38] to elucidate the role of Lewis NH_3 and Brønsted NH_3 in Cu-site redox.

NO and NH_3 consumption was also monitored during the Cummins four-step protocol run over pre-oxidized catalysts (experimental protocol in Fig. 2b) [51]. First, 200 ppm NO and 10% were O_2 were passed through the catalyst, followed by introduction of 200 ppm NH_3. In step-3, NO was removed to probe NH_3 oxidation rates, and step-4 involved titration of pre-stored NH_3 using 200 ppm NO and 10% O_2. The four-step protocol was also performed with 1000 ppm NO and 1000 ppm NH_3 in 10% O_2, to study the influence of feed concentration on SCR and oxidation rates.

All NH_3-TPD experiments were conducted at a total flow rate of 26 SLPM, corresponding to a GHSV of approximately 40,000 h^{-1}. All SCR experiments were conducted in the presence of 7% H_2O and 8% CO_2 in balance N_2 at a total flow rate of 39 SLPM, corresponding to a GHSV of approximately 60,000 h^{-1}. The effluent gas composition for all experiments was analyzed by a high-speed MKS MultiGas 2030 FTIR.

3. Kinetic model and results

The kinetic model shown in this work builds upon a previously reported framework in [21,24]. In this model formalism, an overarching framework aluminum (Al_f) site is considered that includes ZH, ZCuOH, Z_2Cu and ZCu configurations. Details on the surface species considered in the mean-field kinetic model and the conservation equations utilized in the 1-D plug-flow reactor (PFR) model are reported in [21,24].

The number densities of ZH (Brønsted acid), ZCuOH and Z_2Cu sites were estimated experimentally from wet NO + NH_3 titration, dry NO_2 TPD and NH_3 TPD experiments [24]. The catalyst considered in the present work consists of ~2.27 wt% total reducible Cu^{II} sites (corresponding to ~0.36 Cu per CHA cage), with ~80% in the nominally ZCuOH configuration in the degreened state. Minor changes in number of reducible Cu^{II} sites upon hydrothermal aging relative to the measured Cu loading indicate negligible amounts of extra-framework CuO_x species present on the catalyst. Integral NO_2 formation, N_2 formation and NO consumption during redox experiments is normalized to this measured number density of reducible Cu^{II} sites. The oxidation state of all Cu configurations (except ZCu and $ZCuNH_3$) in reaction equations is implicitly defined as + 2.

3.1. Reduction of Cu^{II} sites by NO

Exposure of framework coordinated Cu^{II} ions in Cu-SSZ-13 to NO can lead to the reduction of a portion of these Cu^{II} ions to Cu^{I}, with the resulting formation of surface nitrites and gas-phase NO_2 [34,38]. Reduction of Cu^{II} ions in NO was investigated by flowing NO isothermally over a pre-oxidized catalyst in the degreened state between 200 °C and 450 °C. Fig. 3a demonstrates NO_2 formation beginning at 300 °C, with a further increase at 400 °C. The reversible nature of Cu^{II} reduction in presence of NO (due to Cu^{I} re-oxidation by surface nitrites or NO_2) leads to non-monotonic integral NO_2 formation as a function of temperature (Fig. 3b). Decreased NO_2 formation above 350 °C indicates higher apparent activation energies for the re-oxidation of Cu^{I} ions by NO_2 or nitrites relative to the reduction of Cu^{II} ions by NO. Transient NO_2 formation at additional temperatures and further description of the experimental results can be found in [38].

NO oxidation to NO_2 involves a two-electron transfer, requiring two Cu^{II} ions in proximity or highly mobile intermediate species. Verma et al. [32] have previously demonstrated that oxygen-bridged dimeric Cu^{II} configurations (such as $Z_2Cu_2O_2$) are the active sites for NO oxidation to NO_2 under dry conditions. Dimeric Cu^{II} sites are also expected to catalyze NO oxidation in presence of H_2O [34]. Furthermore, NO can reduce monomeric ZCuOH sites to form mobile HONO intermediates that subsequently decompose to produce gas-phase NO_2 [26].

The number of NO_2 molecules formed per Cu^{II} site reduced is dependent on the stoichiometry of the Cu^{II} configuration, ranging from

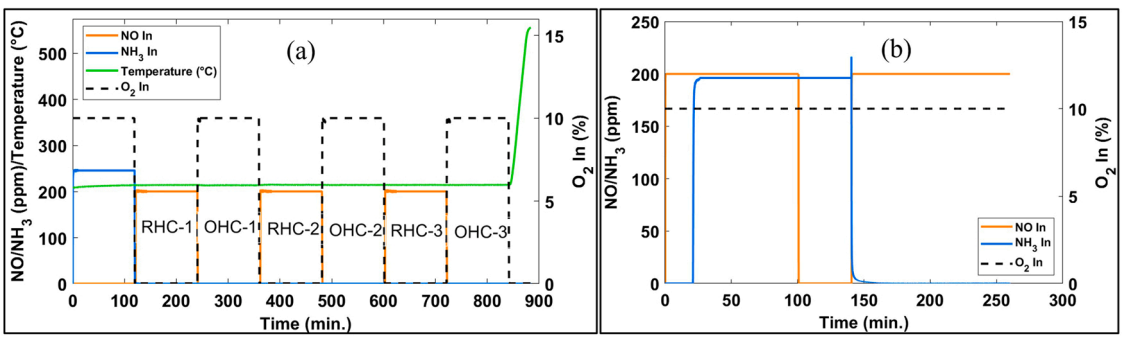

Fig. 2. (a) Experimental protocol for NH_3-adsorption followed by three redox cycles with NO/O_2 and TPD. (b) Isothermal four-step experimental protocol.

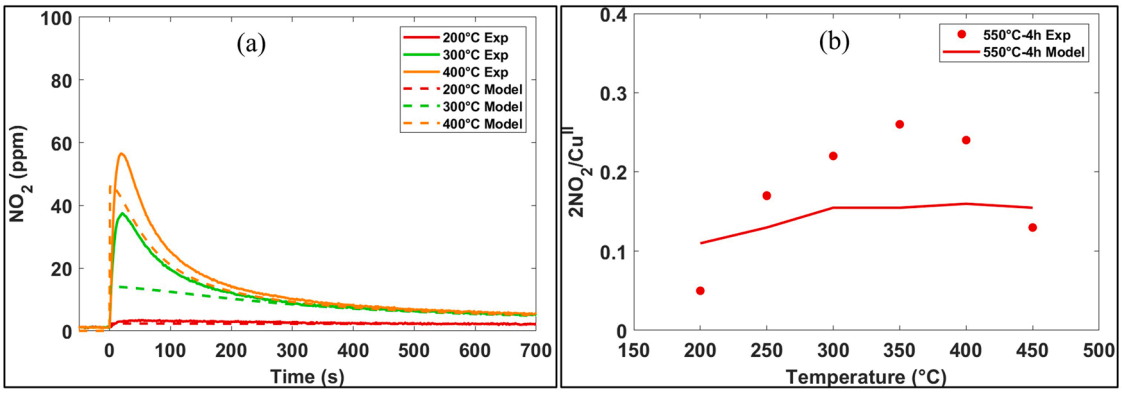

Fig. 3. (a) Transient and (b) Integral NO_2 formation during NO titration of Cu^{II} sites on a degreened catalyst. GHSV: 40,000 h^{-1}.

0.5 NO_2/Cu^{II} (Eqs. (1) and (2)) to 1 NO_2/Cu^{II} (Eq. (3)) for previously reported stable hydroxylated and non-hydroxylated Cu^{II} dimer configurations [15,47].

$$Z_2Cu_2O + NO \leftrightarrow 2ZCu + NO_2 \quad (1)$$

$$Z_2Cu_2O_2H_2 + NO \leftrightarrow 2ZCu + NO_2 + H_2O \quad (2)$$

$$Z_2Cu_2O_2 + 2NO \leftrightarrow 2ZCu + 2NO_2 \quad (3)$$

$NO + NH_3$ titration experiments following NO titration were utilized to confirm the NO-only RHC reaction stoichiometry (for a known $NO + NH_3$ RHC stoichiometry of one N_2/Cu^{II} [21]). Integral N_2/Cu^{II} values from these NH_3-initiated $NO + NH_3$ titration experiments (RHC-a in Fig. 1) on a degreened catalyst at various axial locations are shown in Fig. 4a, indicating that the amount of N_2 formed during RHC-a decreases with increasing temperature, associated with the pre-reduction of Cu^{II} sites in NO. Integral N_2 values at 400 °C are 25–30% lower than at 200 °C. Fig. 3b demonstrates that this decrease in integral N_2 is nearly equal to two times the integral NO_2 produced during preceding NO titration experiments. This stoichiometry suggests the involvement of two proximal ZCuOH sites and mono (μ-oxo) dicopper (II) species in catalyzing NO-only RHC. Fig. S1a in Supporting Information further confirms that the sum of integral N_2 from $NO + NH_3$ titration and two times the integral NO_2 produced from NO titration is constant as a function of temperature, representing the total amount of Cu reduced during this protocol.

Mono (μ-oxo) dicopper (II) species (Z_2Cu_2O) or their partially hydrated dimer form ($Z_2Cu_2O_2H_2$) have been studied extensively in literature in the context of partial methane oxidation (PMO) to methanol [15,46–49]. Khurana et al. [35] recently suggested that these two dimeric Cu^{II} configurations (formed during thermal dehydration of hydrated Cu^{II} complexes) represent likely active site candidates for NO oxidation under dry conditions, consistent with the integral calculations reported in this work. These two dimeric Cu^{II} configurations likely exist in dynamic equilibrium with two proximal monomeric ZCuOH configurations, mediated by H_2O pressure and temperature (Eq. (4)).

$$Z_2Cu_2O + H_2O \leftrightarrow Z_2Cu_2O_2H_2 \leftrightarrow 2ZCuOH \quad (4)$$

The redox model framework reported in our previous work assumes all framework coordinated Cu^{II} ions exist as either monomeric Z_2Cu or ZCuOH sites outside of SCR conditions [21]. In this work, reaction R1 (Table 1) is used to represent reversible NO titration over two proximal ZCuOH sites, which may serve as precursors to dimeric Cu^{II} configurations formed upon dehydration [13,35]. Forward and reverse rates are assumed to be second order in ZCuOH and ZCu number densities respectively. Estimation of rate constants enables qualitative predictions of the transient and integral NO_2 formation during NO titration (Fig. 3), along with the decrease in integral N_2 formation during subsequent $NO + NH_3$ titration above 300 °C (Fig. 4). The resulting forward activation energy associated with the reduction of ZCuOH sites by NO is consistent with density functional theory (DFT) reported values of ~37 kJ/mol [52].

We have previously reported that the extent of NO oxidation and reduction of Cu^{II} sites by NO (in presence of H_2O) decreases upon hydrothermal aging [38,45], indicating a concomitant decrease in the number density of two proximal ZCuOH and/or dimeric Cu^{II} sites. This leads to an increase in the proportion of Cu^{II} sites reduced during subsequent $NO + NH_3$ titration on the hydrothermally aged catalyst above 250 °C, as shown in Fig. 4b. The impact of hydrothermal aging is effectively described by combining the NO-only RHC model reported in this work with a Cu-site transformation hydrothermal aging model [24], and a $NO + NH_3$ RHC model over ZCuOH and Z_2Cu sites [21].

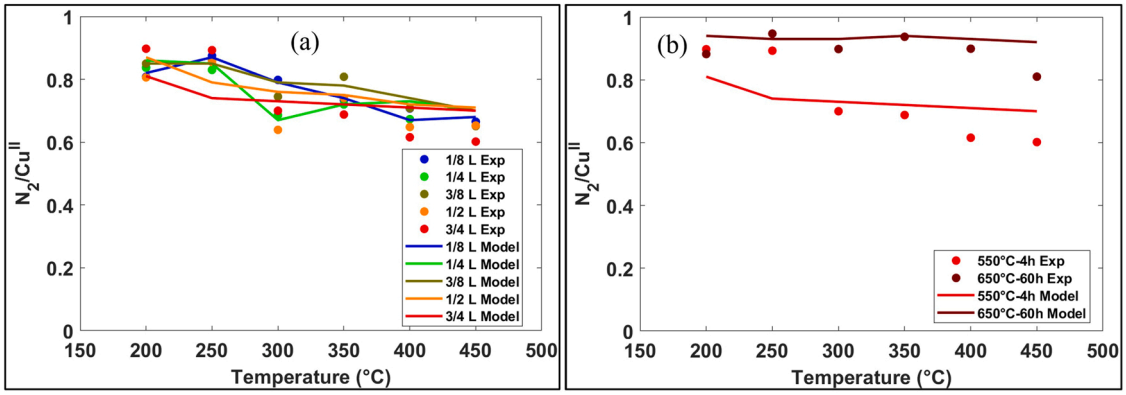

Fig. 4. Integral N_2 formation during $NO + NH_3$ titration of Cu^{II} sites (RHC-a of ten-step TRCR protocol) as a function of (a) Intra-catalyst location on the degreened catalyst, and (b) Hydrothermal age at 3/4 L intra-catalyst location. 1/8 L corresponds to a GHSV of 320,000 h^{-1} and 3/4 L corresponds to a GHSV of 53,000 h^{-1}.

Table 1
NO-only RHC (R1) and NH_3-only RHC (R2) Kinetics.

Reaction	Rate Expression	A Unit	A Value	Ea (kJ/mol)
$2ZCuOH + NO \leftrightarrow 2ZCu + NO_2 + H_2O$	$r_{NO_{RHC}} = k_{NO_{RHC}} y_{NO} (\frac{\theta_{ZCuOH}}{\theta_{ZCuOH_i}})^2 \Omega^2_{ZCuOH} - k_{NO2_{OHC}} y_{NO_2} (\frac{\theta_{ZCu}}{0.5\theta_{Z_2Cu_i} + \theta_{ZCuOH_i}})^2 \Omega^2_{ZCu}$	m^3/mol_{wc}-s	$A_f = 25.62$ $A_b = 7.07E+03$	$E_f = 41.6$ $E_b = 33.3$
$3ZCuOH + NH_3 \rightarrow 3ZCu + 0.5N_2 + 3H_2O$	$r_{NH3_{RHC}} = k_{NH3_{RHC}} y_{NH_3} (\frac{\theta_{ZCuOH}}{\theta_{ZCuOH_i}})^2 \Omega^2_{ZCuOH}$	m^3/mol_{wc}-s	1.69E+04	54

3.2. Reduction of Cu^{II} sites by NH_3

Reduction of Cu^{II} sites in NH_3 was investigated by flowing NH_3 isothermally over pre-oxidized degreened and hydrothermally aged catalysts between 200 °C and 450 °C. N_2 evolution associated with Cu^{II} reduction is observed starting at temperatures above 250 °C (Fig. S2 in Supporting Information). N_2 formation rates and integral N_2 values increase with temperature and decrease upon hydrothermal aging (Fig. 5). The influence of hydrothermal aging is consistent with the involvement of ZCuOH and/or dimeric Cu^{II} sites. Transient N_2 formation at additional temperatures and further description of the experimental results can be found in [38].

NH_3 oxidation to N_2 involves a three-electron transfer per NH_3 molecule. At temperatures below 350 °C, NH_3-solvated Cu^{II} sites can reduce following the stoichiometries shown in Eqs. (5) and (6) for ZCuOH and $Z_2Cu_2O_2H$ configurations respectively. Analogously, at higher temperatures, framework coordinated Cu^{II} sites can reduce following stoichiometries shown in Eqs. (7) and (8). Alternate N_2/Cu^{II} stoichiometries for NH_3 titration of Cu^{II} sites (such as one N_2/Cu^{II}) involve the formation of H_2 [42].

$$3ZCuOHNH_3 + NH_3 \rightarrow 3ZCuNH_3 + 0.5N_2 + 3H_2O \quad (5)$$

$$Z_2Cu_2O_2H(NH_3)_2 + NH_3 \rightarrow 2ZCuNH_3 + 0.5N_2 + 2H_2O \quad (6)$$

$$3ZCuOH + NH_3 \rightarrow 3ZCu + 0.5N_2 + 3H_2O \quad (7)$$

$$Z_2Cu_2O_2H + NH_3 \rightarrow 2ZCu + 0.5N_2 + 2H_2O \quad (8)$$

$NO + NH_3$ titration experiments following NH_3 titration were utilized to confirm the NH_3-only RHC reaction stoichiometry. Integral N_2/Cu^{II} values from NO-initiated $NO + NH_3$ titration experiments (RHC-c in Fig. 1a) on the degreened catalyst were reported in detail in our previous studies [21,38], demonstrating that the amount of N_2 formed during RHC-c significantly decreases with increasing temperature, associated with the pre-reduction of Cu^{II} sites in NH_3. RHC-c integral N_2 values at 400 °C are 70–75% lower than at 200 °C. Fig. 6b demonstrates that this decrease in integral N_2 is nearly equal to six times the integral N_2 produced during preceding NH_3 titration experiments on the degreened catalyst. Fig. S1b in Supporting Information further confirms that the sum of integral N_2 from $NO + NH_3$ titration and six times the integral N_2 produced from NH_3 titration is approximately constant as a function of temperature, representing the total amount of Cu reduced during this protocol.

NH_3 titration of nominally ZCuOH sites is represented by reaction R2 (Table 1) in the redox model framework. Model studies indicated that transient N_2 evolution during NH_3-only RHC is best represented by a rate expression that is second order in ZCuOH number density (similar fits were also observed using third order rates). Identification of rate constant parameters enables qualitative descriptions of the transient and integral N_2 formation as a function of temperature and hydrothermal aging (Fig. 5 and Fig. 6), with an estimated activation energy of ~54 kJ/mol.

Overestimation of transient and integral N_2 formation at 450 °C may be associated with auto-reduction of Cu^{II} sites, not considered in the redox model framework. Underprediction of integral N_2/Cu^{II} below 350 °C is associated with reduction of NH_3-solvated Cu^{II} sites, and can be reconciled upon inclusion of Eq. (5). N_2 measurements shown here indicate analogous adsorbed NH_3 and gas-phase NH_3 routes for both NO + NH_3 RHC [21,53], and NH_3-only RHC. Two distinct routes for NH_3-only RHC also rationalize the bi-modal NH_3 conversion observed as a function of temperature during NH_3 oxidation experiments on Cu-SSZ-13 [45]. Mechanistic similarities and differences between Cu^{II} reduction pathways in presence of NO and/or NH_3 are discussed further in Section 4. Table 1 summarizes the NO-only RHC and NH_3-only RHC reaction kinetics.

3.3. Oxidation of partially solvated and NH_3-free Cu^{I} sites by O_2

Oxidation of NH_3-solvated Cu^{I} sites ($ZCu(NH_3)_2$) in presence of O_2 (relevant to low temperature standard SCR) has been demonstrated to proceed over pairs of Cu^{I} sites, leading to the formation of NH_3-solvated Cu^{II} dimers [16,17]. In our previous work, we reported on a kinetic model for the oxidation NH_3-solvated Cu^{I} pairs, along with the subsequent reduction of NH_3-solvated Cu^{II} dimers in presence of NO [21]. Increasing temperatures leads to desorption of NH_3 from Cu^{I} ions, forming partially solvated ($ZCuNH_3$) and framework coordinated ZCu sites [24].

Oxidation rates over these Cu^{I} configurations were investigated by flowing NO and O_2 isothermally over pre-reduced degreened and hydrothermally aged catalysts between 200 °C and 450 °C (OHC-a in

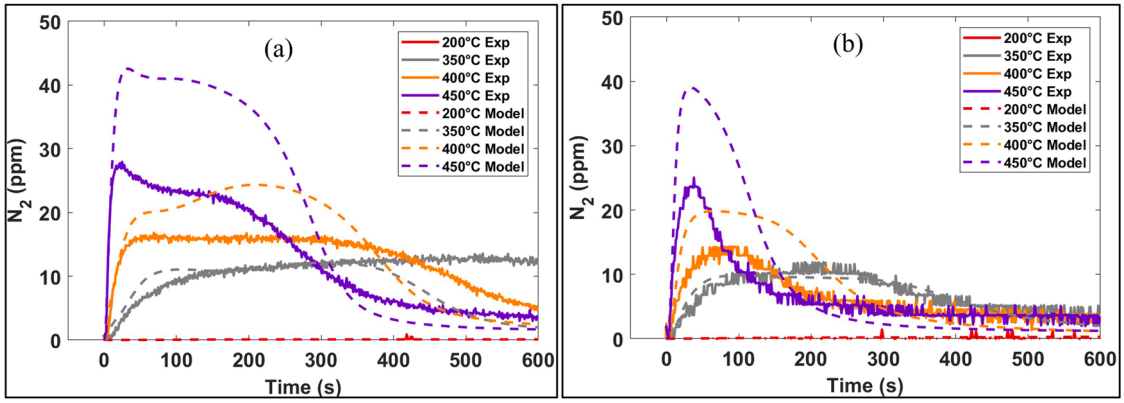

Fig. 5. Transient N_2 formation during NH_3 titration of Cu^{II} sites on (a) degreened and (b) hydrothermally aged catalyst. GHSV: 53,000 h^{-1}.

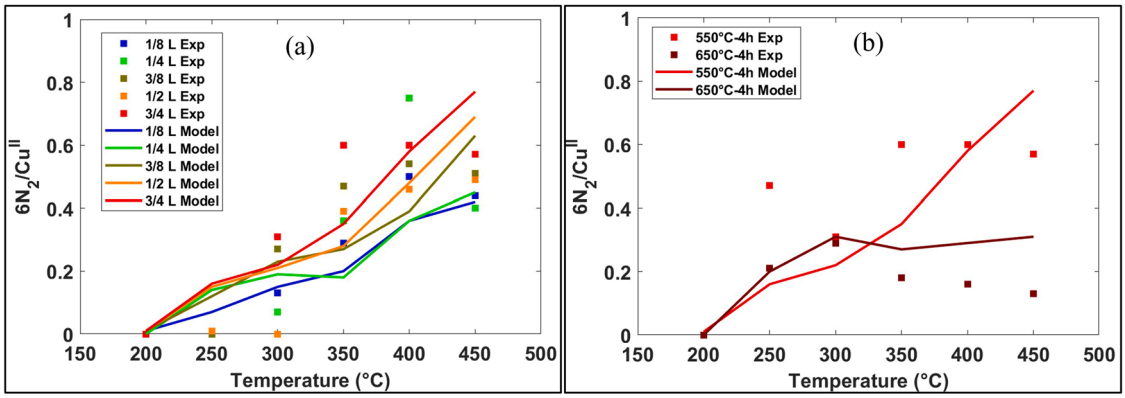

Fig. 6. Integral N_2 formation during NH_3 titration of Cu^{II} sites as a function of (a) Intra-catalyst location on the degreened catalyst, and (b) Hydrothermal age at 3/4 L intra-catalyst location. 1/8 L corresponds to a GHSV of 320,000 h^{-1} and 3/4 L corresponds to a GHSV of 53,000 h^{-1}.

Fig. 1). NO was included due to its relevance for standard SCR conditions, enabling detection and quantification of N_2 evolution. Fig. 7 and Fig. 8 plot the integral and transient N_2 evolution respectively during OHC-a. Initial N_2 formation rates (derived from Fig. 8) increase with increasing temperature, confirming the activated nature of Cu^I oxidation. Integral N_2/Cu^{II} values are in the range of 2–2.5 at 200 °C, and decrease monotonically with increasing temperatures to ~0.4–0.5 at 450 °C (Fig. 7). Furthermore, integral N_2/Cu^{II} values are lower for the hydrothermally aged catalyst relative to the degreened catalyst at all temperatures (Fig. 7b).

3.3.1. *Intrinsic OHC pathways*

Oxidation of $ZCuNH_3$ and ZCu sites in presence of NO and O_2 can proceed via multiple pathways. Cu-nitrate intermediates have been proposed to form during this re-oxidation step [29], inhibited by the presence of H_2O [7]. No evidence of Cu-nitrate formation was found during the OHC-a experiments conducted in this work in presence of 5% H_2O. Recent titration and spectroscopic experiments indicate that O_2 alone can oxidize all Cu^I sites, and no N_2 evolution is observed during this oxidation process [26,38,54]. The role of Brønsted acid sites in the oxidation step requires further clarification.

Bregante et al. [49] utilized X-ray absorption spectroscopy (XAS) and time-resolved resonance Raman spectroscopy to detect the structural evolution of Cu^{II} complexes from trans-μ-1,2 peroxo dicopper(II) species to mono (μ-oxo) dicopper(II) species following oxidation of Cu^I ions in O_2. This can be represented stoichiometrically by Eqs. (9) and (10).

$$2ZCu + O_2 \leftrightarrow Z_2Cu_2O_2 \quad (9)$$

$$Z_2Cu_2O_2 \leftrightarrow Z_2Cu_2O + 0.5O_2 \quad (10)$$

Z_2Cu_2O complexes can partially hydrolyze to recover two-proximal monomeric ZCuOH sites, following Eq. (4). Eq. (9) requires the presence of pairs of Cu^I ions in proximity. Analogous oxidation reactions can be written for $ZCuNH_3$ complexes instead of ZCu. Usberti et al. [26] have shown that framework coordinated Cu^I ions can oxidize completely at 150 °C in presence of O_2, while NH_3-solvation may inhibit Cu^I oxidation rates [56].

Kubota et al. [54] have utilized infrared spectroscopy to detect the consumption of Brønsted acid sites during oxidation of Cu^I ions in presence of O_2. This can be rationalized by the reverse hydrolysis of ZCuOH sites formed during OHC, leading to the consumption of Brønsted acid sites and formation of Z_2Cu sites. In Eq. (11), x represents the NH_3 coordination on ZCuOH sites, and y represents the NH_3 coordination on ZH sites. Hu et al. [20] have demonstrated that this reaction is driven in the backward direction during RHC, due to the dimerization and reduction of NH_3-solvated ZCuOH sites in presence of NO. In absence of NO during OHC, it is suggested that this reaction may be driven forward, leading to the consumption of Brønsted NH_3. Further evidence for this is presented in Section 3.3.4.

$$ZCuOH(NH_3)_x + ZH(NH_3)_y \leftrightarrow Z_2Cu(NH_3)_{x+y} + H_2O \quad (11)$$

3.3.2. *Consumption of NO and Brønsted NH_3*

Framework coordinated ZCuOH sites formed during OHC can subsequently reduce in presence of gas-phase NO, leading to the formation of mobile HONO intermediates that can react with Brønsted NH_3 or gas-phase NH_3 via energetically favorable pathways involving nitrosyl or nitrosamine intermediates [18,26,53–55].

$$ZCuOH + NO \leftrightarrow ZCu + HONO \quad (12)$$

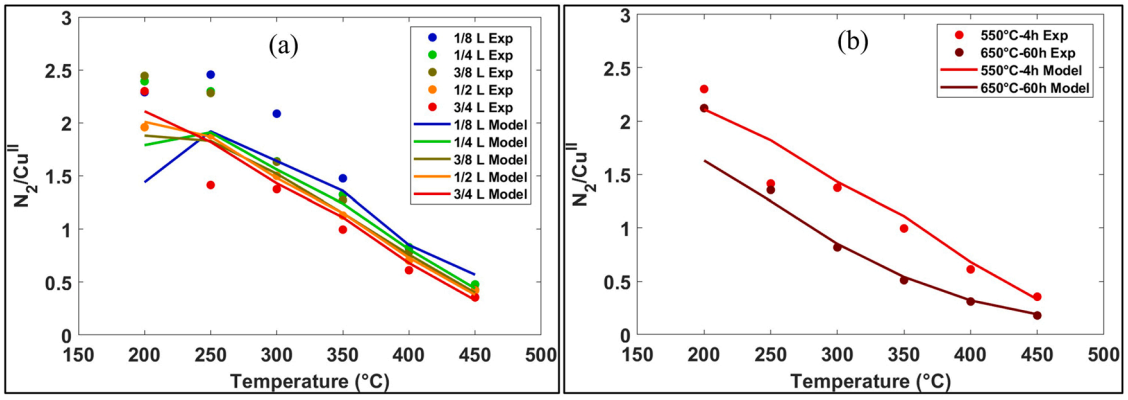

Fig. 7. Integral N_2 formation during NO + O_2 titration of Cu^I sites (OHC-a of ten-step TRCR protocol) as a function of (a) Intra-catalyst location on the degreened catalyst, and (b) Hydrothermal age at 3/4 L intra-catalyst location. 1/8 L corresponds to a GHSV of 320,000 h^{-1} and 3/4 L corresponds to a GHSV of 53,000 h^{-1}.

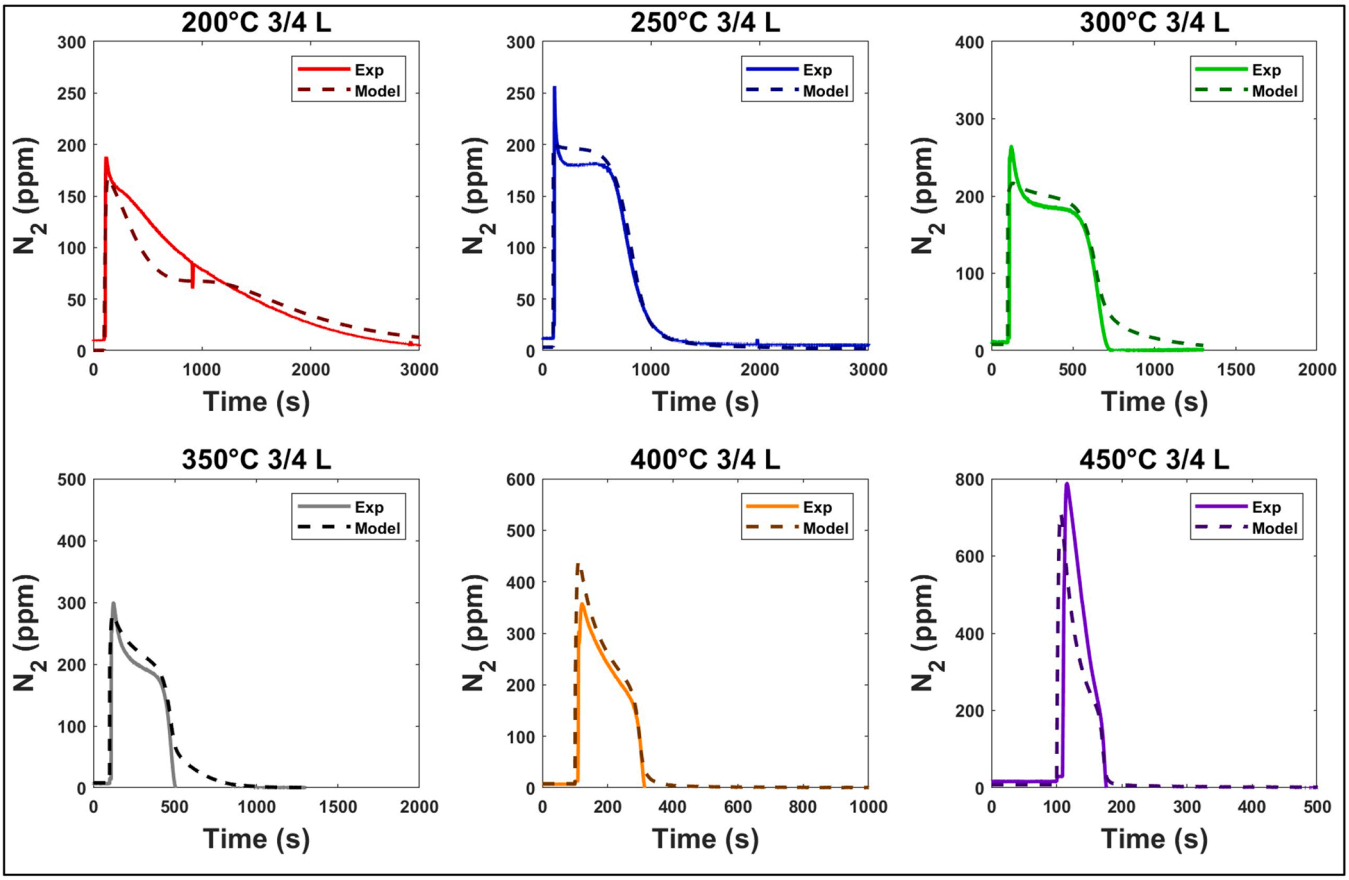

Fig. 8. Transient N_2 formation during NO + O_2 titration of Cu^I sites (OHC-a of ten-step TRCR protocol) on a degreened catalyst. GHSV: 53,000 h^{-1}.

$$HONO + ZNH_4 \rightarrow ZH + N_2 + 2H_2O \quad (13)$$

Eqs. (12)-(13) help rationalize the increased consumption of Brønsted NH_3 in the second reduction half cycle (RHC) following oxidation in O_2 relative to the first reduction half cycle [26,38,54]. In absence of NH_3-solvated Cu^{II} complexes, HONO intermediates can diffuse through the zeolite to react with Brønsted NH_3. NH_3-solvated ZCuOH and Z_2Cu sites formed during OHC would subsequently dimerize and reduce in presence of NO, without the additional consumption of Brønsted NH_3 [25].

3.3.3. Global OHC model

As N_2 is not an expected product of Cu^I oxidation, N_2 measurements during exposure of Cu^I ions to a mixture of NO and O_2 cannot be utilized to directly quantify intrinsic rates of Cu^I oxidation by O_2. In the redox model framework, irreversible global reactions are derived to predict transient and integral N_2 formation during exposure of Cu^I ions to a mixture of of NO and O_2. These global reactions represent combinations of oxidation and subsequent reduction reactions with and without the consumption of Brønsted acid sites.

Direct oxidation of ZCu sites to framework coordinated ZCuOH sites is represented as a combination of Eq. (9), Eq. (10) and Eq. (4), labeled as OHC6. Analogous direct oxidation of $ZCuNH_3$ sites was not necessary to predict experimental data, indicating inhibited OHC rates in presence of surface NH_3 [56].

Equation (4) + Equation (9) + Equation (10) = OHC6

$$\textbf{OHC6}: 2ZCu + 0.5O_2 + H_2O \rightarrow 2ZCuOH \quad (14)$$

To account for the consumption of Brønsted acid sites during OHC, the reverse hydrolysis of ZCuOH sites is considered, resulting in OHC7.

Equation (4) + Equation (9) + Equation (10) + Equation (11) = OHC7

$$\textbf{OHC7}: 2ZCu + 0.5O_2 + 2ZH \rightarrow 2Z_2Cu + H_2O \quad (15)$$

The repartitioning of Brønsted NH_3 to Lewis NH_3 during the oxidation of Cu^I ions in O_2 (discussed in Section 3.3.4) is represented by OHC5.

$$\textbf{OHC5}: ZCuNH_3 + ZNH_4 + O_2 \rightarrow ZCuOHNH_3 + ZH + N_2 + H_2O \quad (16)$$

NO consumption during exposure of Cu^I ions to a mixture of NO and O_2 is associated with the reduction of Cu^{II} ions (formed during OHC), via NO + NH_3 RHC pathways consuming Lewis NH_3 and Brønsted NH_3. While RHC pathways consuming Lewis NH_3 are included in the NO + NH_3 RHC model (see reference [21]), RHC pathways consuming Brønsted NH_3 (via Eqs. (12) and (13)) are indirectly considered in the global OHC model to explain the over stoichiometric consumption of NO (i.e. $N_2/Cu^{II} > 1$) reported in Fig. 7. The resulting global OHC reaction is labeled as OHC4.

Equation (4) + Equation (9) + Equation (10) + Equation (12) + Equation (13) = OHC4

$$\textbf{OHC4}: ZCu + ZNH_4 + NO + 0.5O_2 \rightarrow ZCuOH + ZH + N_2 + H_2O \quad (17)$$

Analogous global OHC reactions are written to account for the oxidation of $ZCuNH_3$ complexes (OHC2) and consumption of physisorbed NH_3 on Brønsted acid sites (OHC3).

OHC2 : $ZCuNH_3 + ZNH_4 + NO + 0.5O_2 \rightarrow ZCuOHNH_3 + ZH + N_2 + H_2O$ (18)

OHC3 : $ZCu + ZNH_4NH_3 + NO + 0.5O_2 \rightarrow ZCuOHNH_3 + ZH + N_2 + H_2O$ (19)

The six global OHC reactions derived here are necessary to describe measured N_2 formation during the OHC-a step of the TRCR protocol. Table 2 shows a comparison of the various global OHC reactions included in the redox model, considering intrinsic OHC pathways along with subsequent NO titration of Cu^{II} sites and consumption of Brønsted NH_3. The N_2/Cu^{II} ratio provides an estimate of the expected N_2 production from the global OHC reaction stoichiometry during OHC-a, along with a measure of the expected N_2 formation from subsequent NO titration of NH_3-solvated Cu^{II} sites (in parenthesis). For instance, OHC2 and OHC3 reactions lead to the formation of two N_2 per Cu^{II} in total, associated with the formation and reduction of NH_3-solvated ZCuOH sites. Intrinsic OHC pathways (OHC6 and OHC7) do not consume NO or produce N_2.

Activation energies for OHC2, OHC3 and OHC4 reactions are set to 95.6 kJ/mol, consistent with estimates from literature for samples with relatively high Cu loadings [57], and values reported by us previously for the NO titration of NH_3-solvated Cu^{II} dimers [21]. Transient and integral N_2 formation data during the OHC-a step of the TRCR protocol was utilized to derive the remaining rate constant parameters associated with Eqs. (14)-(19). Model studies indicated that transient N_2 evolution during OHC-a is best represented by rate expressions that are second order in ZCu number density, concordant with Eq. (9) being the rate determining step. Integral N_2/Cu^{II} values estimated from the resulting model (Fig. 7) are consistent with measurements as a function of temperature and hydrothermal aging. Similarly, transient N_2 predictions are consistent with measured transient N_2 during OHC-a (Fig. 8). Underestimation of integral N_2/Cu^{II} at 200 °C and high GHSV (1/8 L) represents a model error associated with competition from auto-reduction of NH_3-solvated Cu^{II} dimers, as discussed in reference [21].

Fig. S3 in Supporting Information plots the transient N_2 formation during OHC-a on the hydrothermally aged catalyst. Initial N_2 formation rates on the hydrothermally aged catalyst are similar to the degreened catalyst at low temperatures, while significantly higher rates are measured and predicted at 450 °C on the degreened catalyst, associated with increased NH_3-only RHC rates. Redox turnover rates during OHC-a are shown in Fig. S4 and Fig. S5 in Supporting Information.

At low temperatures, the presence of $ZCuNH_3$ and ZNH_4NH_3 complexes leads to significant contributions of OHC2 and OHC3 reactions (along with oxidation of $ZCu(NH_3)_2$ pairs) during OHC-a, followed by subsequent NO titration of the resulting $ZCuOHNH_3$ complexes, producing two N_2/Cu^{II}. With increasing temperatures, NH_3 de-solvation leads to increased contributions from OHC4, OHC6 and OHC7, forming framework coordinated ZCuOH and Z_2Cu sites. While OHC4 produces one N_2/Cu^{II}, no N_2 is produced from OHC6 and OHC7. Temperature-dependent transitions in global OHC reactions quantitatively rationalize transient and integral N_2 formation during exposure of NH_3-solvated and framework coordinated Cu^{I} ions to a mixture of NO and O_2. Lower integral N_2/Cu^{II} upon hydrothermal aging is associated with decreased Brønsted acidity on the hydrothermally aged catalyst, leading to decreased NO consumption via OHC2, OHC3 and OHC4 reactions.

Table 2
Comparison of Global OHC reactions in Redox Model.

Global OHC reaction	Cu^{I} Reactant	Consumption of NO	Consumption of Brønsted Acid Sites	Cu^{II} Product	N_2/Cu^{II} during OHC-a
OHC2	$ZCuNH_3$	Yes	No	$ZCuOHNH_3$	1(+1)
OHC3	ZCu	Yes	No	$ZCuOHNH_3$	1(+1)
OHC4	ZCu	Yes	No	ZCuOH	1
OHC5	$ZCuNH_3$	No	Yes	$ZCuOHNH_3$	0.5 (+1)
OHC6	ZCu	No	No	ZCuOH	0
OHC7	ZCu	No	Yes	Z_2Cu	0

3.3.4. *Repartitioning of NH_3 during OHC*

NH_3 TPD experiments described in Section 2.2 were utilized to validate redox model predictions and identify rate parameters associated with the repartitioning of NH_3 from Brønsted acid sites to Lewis acid sites during OHC. Solid lines in Fig. 9 show the measured NH_3 release as a function of temperature for four TPD experiments on a degreened catalyst. The baseline NH_3 TPD (red line in Fig. 9) shows two distinct NH_3 release peaks, associated with desorption of NH_3 from Cu^{II} sites (~290 °C) and Brønsted acid sites (~410 °C) [42]. This is effectively described by the NH_3 adsorption-desorption kinetic model reported by us previously [24]. Reduction of NH_3-solvated Cu^{II} sites in presence of NO leads to nearly complete consumption of Lewis NH_3, consistent with NO + NH_3 RHC kinetic model predictions (dashed blue line in Fig. 9) [21].

NH_3 TPD after re-oxidation of Cu^{I} ions in O_2 demonstrates a decreased NH_3 release above 350 °C and an increased NH_3 release below 350 °C relative to the TPD before re-oxidation (solid green and blue lines in Fig. 9). This indicates a consumption of Brønsted acid sites and/or Brønsted NH_3 during re-oxidation. No evidence of gas-phase NO_2 or surface nitrates was observed during the experiment, ruling out the role of oxidized N-containing surface intermediates or NO_2 in the consumption of Brønsted NH_3. Deka et al. [38] attributed the concomitant increase in NH_3 release below 350 °C to a repartitioning of NH_3 from Brønsted acid sites to Lewis acid sites, consistent with results shown here and with Eq. (11). The transformation of stable Brønsted NH_3 to less stable Lewis NH_3 can be thermodynamically driven by the formation of stable H_2O as a product. The un-activated OHC5 global reaction (Eq. (16)) is utilized in the redox model to describe this NH_3 re-partitioning, and the resulting model predictions are qualitatively consistent with experiments (dashed green line in Fig. 9). Repeated isothermal exposure to NO followed by O_2 leads to complete consumption of Brønsted NH_3 (solid black line in Fig. 9), in agreement with previously reported measurements and rationalized by Eqs. (9)-(13) [26,38].

Similar experiments were also repeated on a catalyst hydrothermally aged at 650 °C for 5 h. Fig. S7 in Supporting Information plots the experimental NH_3-TPD profiles and model predictions, following the same trends as shown in Fig. 9 for the degreened catalyst.

Table 3 summarizes the global OHC reaction kinetics. The stoichiometries represented in Table 3 reflect the apparent second order nature of the global OHC reactions, and the resulting products (for non-intrinsic OHC pathways) assume an equimolar production of ZCuOH and Z_2Cu sites, as they are indistinguishable under SCR conditions. Combining these global OHC reactions with the RHC kinetics reported in Table 1 and reference [21] recovers the well-known global reaction stoichiometries for standard SCR, NO oxidation and NH_3 oxidation reactions.

3.4. *Model validation*

3.4.1. *SCR conversion inflections*

RHC and OHC kinetics reported in this work were validated with SCR steps of the ten-step TRCR protocol shown in Fig. 1. The SCR-b step in this protocol involves flowing NO, NH_3 and O_2 over a catalyst pre-reduced in NO and NH_3. The introduction of O_2 during SCR-b leads to oxidation of Cu^{I} ions, and subsequent reduction in NO and NH_3. Partridge et al. [58] previously observed that the initial N_2 formation rates during these SCR experiments are higher than steady-state N_2 formation rates. This is associated with RHC-OHC rate imbalances, leading to conversion inflections. Initial N_2 transients during SCR-b can provide indirect information on OHC rates [27,58].

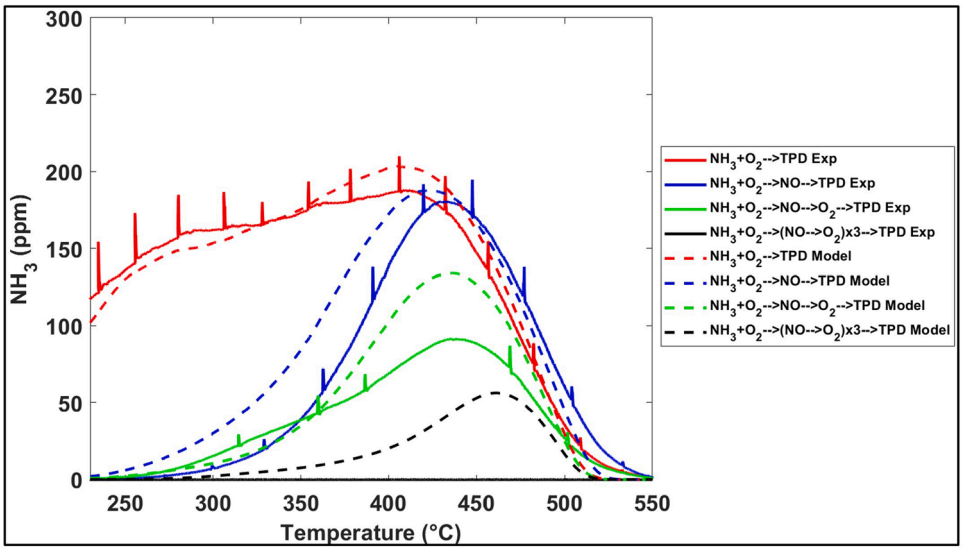

Fig. 9. NH_3 TPD following isothermal reduction-oxidation on a degreened (550 °C-4 h) catalyst. GHSV: 40,000 h^{-1}.

Table 3
Global OHC Kinetics over $ZCuNH_3$ and ZCu Sites.

Reaction	Rate Expression	A Unit	A Value	Ea (kJ/mol)
$2ZCuNH_3 + 2ZNH_4 + 2NO + O_2 \rightarrow ZCuOHNH_3 + Z_2CuNH_3 + ZH + 2N_2 + 3H_2O$	$r_{OHC2} = k_{OHC2} y_{NO} y_{O_2} \theta^2_{ZCuNH_3} \theta^2_{ZNH_4} \Omega_{Alf}$		3.55E+ 15	
$2ZCu + 2ZNH_4NH_3 + 2NO + O_2 \rightarrow ZCuOHNH_3 + Z_2CuNH_3 + ZH + 2N_2 + 3H_2O$	$r_{OHC3} = k_{OHC3} y_{NO} y_{O_2} \theta^2_{ZCu} \theta^2_{ZNH_4NH_3} \Omega_{Alf}$	1/s	1.30E+ 16	95.6
$2ZCu + 2ZNH_4 + 2NO + O_2 \rightarrow ZCuOH + Z_2Cu + ZH + 2N_2 + 3H_2O$	$r_{OHC4} = k_{OHC4} y_{NO} y_{O_2} \theta^2_{ZCu} \theta^2_{ZNH_4} \Omega_{Alf}$		1.17E+ 17	
$2ZCuNH_3 + 2ZNH_4 + 2O_2 \rightarrow ZCuOHNH_3 + Z_2CuNH_3 + ZH + N_2 + 3H_2O$	$r_{OHC5} = k_{OHC5} y^2_{O_2} \theta^2_{ZCuNH_3} \theta^2_{ZNH_4} \Omega_{Alf}$		7.4	0
$2ZCu + 0.5O_2 + H_2O \rightarrow 2ZCuOH$	$r_{OHC6} = k_{OHC6} y^{0.5}_{O_2} \left(\frac{\theta_{ZCu}}{0.5\theta_{Z_2Cu_i} + \theta_{ZCuOH_i}}\right)^2 \Omega^2_{ZCu}$	m^3/mol_{wc}-s	0.7	33.3
$2ZCu + 0.5O_2 + 2ZH \rightarrow 2Z_2Cu + H_2O$	$r_{OHC7} = k_{OHC7} y^{0.5}_{O_2} \left(\frac{\theta_{ZCu}\theta_{ZH}(0.5\theta_{Z_2Cu_i})}{\theta_{ZCuOH_i}(0.5\theta_{Z_2Cu_i} + \theta_{ZCuOH_i})}\right)^2 \Omega^2_{ZCu}$		0.35	

Fig. 10 plots the N_2 formation during SCR-b as a function of temperature and hydrothermal aging. Initial N_2 formation rates increase with temperature, associated with increased initial reduction of Cu^{II} ions by gas-phase NH_3 following direct oxidation of Cu^{I} ions in O_2. The higher number density of ZCuOH sites leads to increased NH_3-only RHC rates on the degreened catalyst relative to the hydrothermally aged catalyst, resulting in increased initial N_2 formation rates. Transient N_2 formation during SCR-b is quantitatively predicted by the redox kinetic model (Fig. 10) at all temperatures on the degreened and hydrothermally aged catalysts. Model predicted total RHC and OHC rates during SCR-b are shown in Fig. S9 in Supporting Information.

The SCR-c step in the TRCR protocol involves flowing NO, NH_3 and O_2 over a catalyst pre-oxidized in NO and O_2. The introduction of NH_3 during SCR-c leads to reduction of Cu^{II} ions, and subsequent oxidation in O_2. Similar to SCR-b, initial N_2 formation rates during SCR-c can be higher than steady-state N_2 formation rates, associated with RHC-OHC rate imbalances leading to conversion inflections. Initial N_2 transients during SCR-c can provide information on intrinsic RHC rates [27,58].

Fig. 11 plots the N_2 formation during SCR-c as a function of temperature and hydrothermal aging. Initial N_2 formation rates increase with temperature, associated with increased initial reduction of Cu^{II} ions by NO and/or NH_3. The higher number density of ZCuOH sites leads to

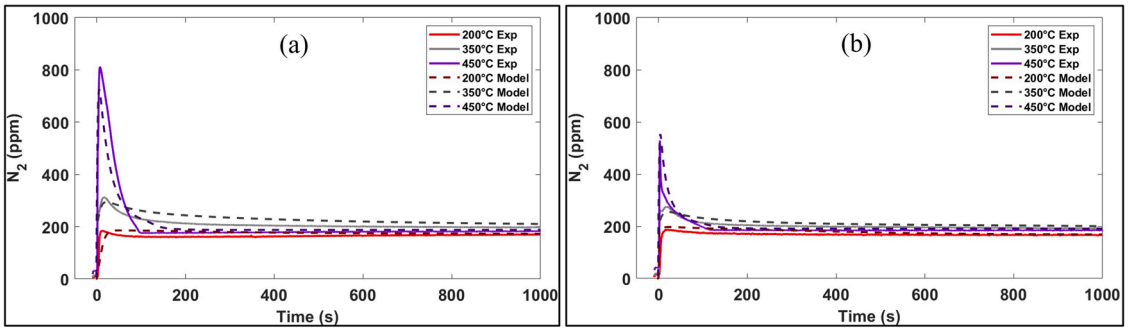

Fig. 10. Transient N_2 formation during standard SCR over a pre-reduced catalyst (SCR-b of ten-step TRCR protocol) in the (a) degreened state and (b) hydrothermally aged state. GHSV: 53,000 h^{-1}.

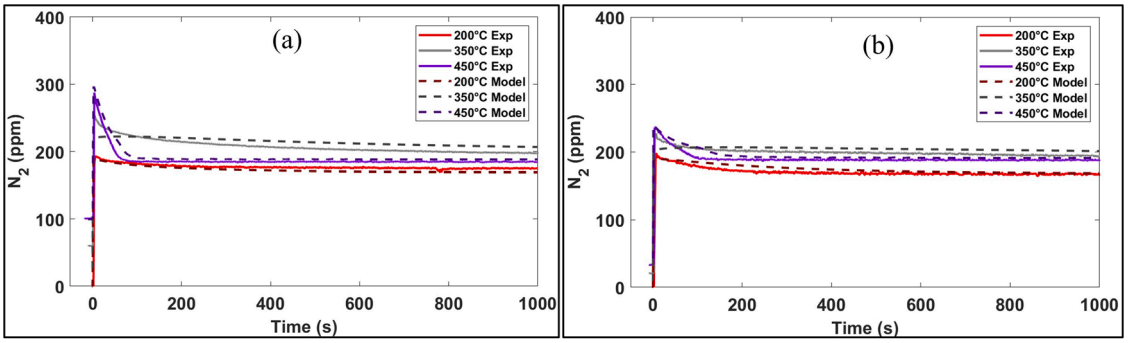

Fig. 11. Transient N_2 formation during standard SCR over a pre-oxidized catalyst (SCR-c of ten-step TRCR protocol) in the (a) degreened state and (b) hydrothermally aged state. GHSV: 53,000 h^{-1}.

increased NH_3-only RHC rates on the degreened catalyst relative to the hydrothermally aged catalyst, resulting in increased initial N_2 formation rates. Transient N_2 formation is quantitatively described by the redox kinetic model. Model predicted total RHC and OHC rates are shown in Fig. S11 in Supporting Information. Increased conversion inflections during SCR-b relative to SCR-c are associated with higher NH_3-only RHC rates at onset of SCR-b compared to SCR-c. This is demonstrated in Fig. S16 in Supporting Information.

The contribution of NH_3-only RHC to N_2 formation during oxidation in presence of O_2 is highlighted in Fig. S12 in Supporting Information. This figure plots the experimental and model predicted N_2 formation during oxidation in O_2 (without NO) on a degreened catalyst pre-reduced in presence of NO and NH_3. No N_2 is measured during oxidation in O_2 below 300 °C, while N_2 formation above 300 °C is quantitatively rationalized in the redox model by NH_3-only RHC occurring from isothermally desorbed gas-phase NH_3.

3.4.2. *Ten-step TRCR protocol*

Model predictions were also compared over the complete ten-step TRCR protocol described in Section 2.1. Fig. 12 plots the transient N_2 formation during this protocol from 200 °C to 450 °C on a degreened catalyst at z/L = 3/4 (GHSV ~ 53,000 h^{-1}). Model predictions (shown as dashed lines in Fig. 12) agree quantitatively with measured N_2 throughout the protocol at all temperatures, demonstrating the validity of the proposed redox framework. Increased integral N_2 formation during OHC-a relative to RHC-a below 400 °C is associated with the consumption of Brønsted NH_3 during OHC-a.

Additional ten-step model results of the transient N_2 formation, NO consumption, Cu^{II} fraction, NH_3 coverage and redox turnover rates over degreened and hydrothermally aged catalysts are described in Section 6 in Supporting Information. Fig. S16 demonstrates the increasing contribution of NH_3-only RHC in the reduction of Cu^{II} ions at high temperatures. Model predicted NO and NH_3 concentrations during the ten-step TRCR protocol agree quantitatively with FTIR measurements at all temperatures (Fig. S20 in Supporting Information). Cu^{II} fraction at steady-state SCR monotonically increases from ~55–60% at 200 °C to ~90–95% at 300 °C (Fig. S21 in Supporting Information). Increasing temperatures further leads to negligible changes in steady-state Cu^{II} fraction, with a minor decrease at 450 °C associated with NH_3-only RHC.

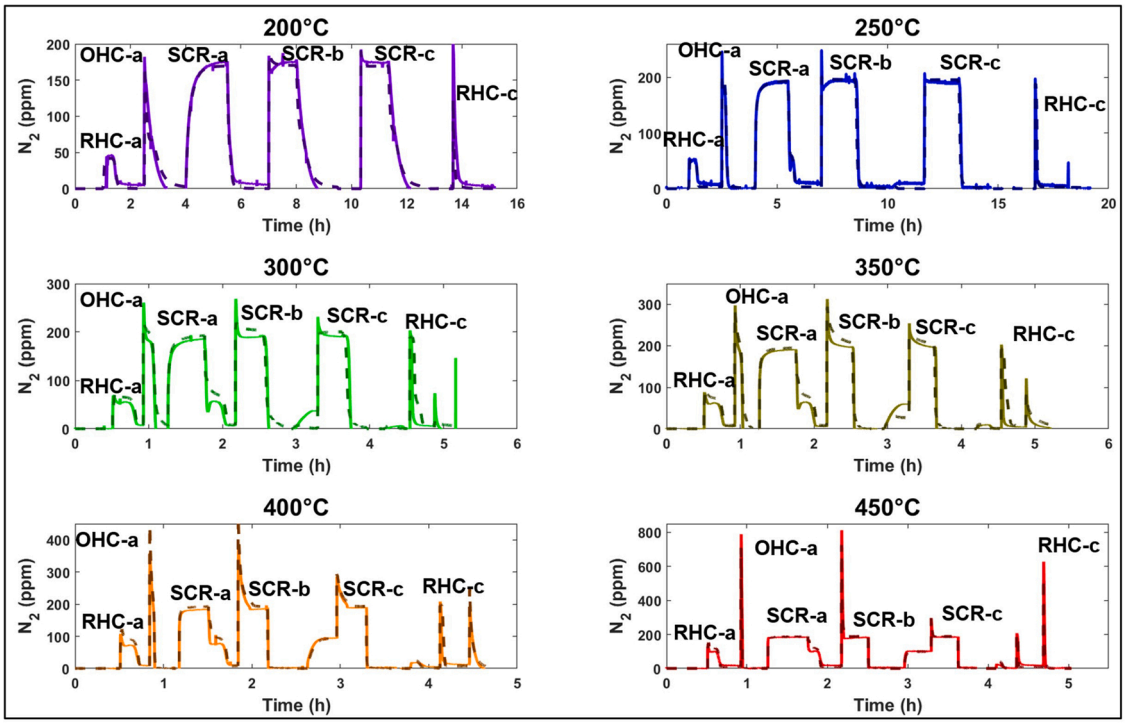

Fig. 12. Transient N_2 formation during ten-step TRCR protocol on a degreened catalyst from 200 °C to 450 °C. Solid lines represent experimental values and dashed lines represent model predictions. GHSV: 53,000 h^{-1}.

Model validation with measured NO and NH_3 concentrations during additional TRCR protocols run between 150 °C and 250 °C is summarized in Section 7 in Supporting Information. Reducing NH_3-solvated Cu^{II} sites with NO instead of NO and NH_3 leads to a decrease in NO consumption during subsequent exposure of Cu^{I} ions to a mixture of NO and O_2 (from ~2 NO/Cu^{II} to ~1 NO/Cu^{II}).

3.4.3. *Four-step protocol*

The Cummins four-step protocol probes the NO oxidation, dynamic NO_x conversion, NH_3 oxidation and NO + O_2 titration functions of an SCR catalyst [51]. Accurate predictions over the four-step protocol enable utilization of kinetic models in transient drive cycle simulations of after treatment catalysts for system conversion efficiency predictions. Fig. 13a plots the NO and NH_3 concentrations during the four-step protocol on a degreened catalyst at 190 °C. Introduction of 200 ppm NH_3 over a pre-oxidized catalyst during step-2 leads to transient NO consumption from standard SCR concomitant with buildup of NH_3 coverage. Incomplete NO conversion is accompanied by NH_3 slip for an equimolar feed of NO and NH_3. Negligible NO and NH_3 oxidation is observed at low temperatures, while NO consumption during step-4 is associated with the titration of NH_3-solvated Cu sites and Brønsted acid sites. Integral NO consumed/Cu^{II} ratios during step-4 at 190 °C are estimated to be ~2.3, identical to the values derived from the OHC-a step of the TRCR protocol at 200 °C (Section 3.3).

Redox model predictions during the four-step protocol at 190 °C on the degreened catalyst are quantitatively consistent with measurements (dashed lines in Fig. 13a). Minor overestimation of step-2 NH_3 slip is associated with parasitic NH_3 oxidation during standard SCR, not considered in the redox model. Hydrothermal aging does not alter the transient NO conversion during step-2 but decreases the extent of parasitic NH_3 oxidation (Fig. 13b). Lower steady-state NH_3 slip relative to NO slip on the hydrothermally aged catalyst is associated with actual feed NH_3 to NO_x ratios less than 1. The loss of Brønsted acidity upon hydrothermal aging leads to decreased NH_3 storage and decreased NO consumption during step-4, described by the redox model.

Increasing the four-step protocol temperature to 430 °C leads to ~15% of the NO being oxidized to NO_2 during step-1 (Fig. 13c). Standard SCR NO conversion is measured to be ~90% during step-2, with complete NH_3 oxidation during step-3. Low NH_3 coverage at 430 °C leads to earlier steady states relative to data at lower temperatures, in line with model predictions. Similarly, model predictions of the influence of increasing NO and NH_3 feed concentrations from 200 ppm to 1000 ppm at a four-step protocol temperature of ~200 °C are consistent with measurements (Fig. 13d).

Additional four-step model results of the steady-state NO conversion as a function of temperature, Cu^{II} fraction, NH_3 coverage and redox turnover rates over degreened and hydrothermally aged catalysts are described in Section 8 in Supporting Information. Cu^{II} fraction during the four-step protocol on the degreened catalyst at 190 °C decreases to ~75% at the end of step-2, and recovers to ~90% at the end of step-4 (Fig. S25 in Supporting Information). Redox reactions occur with identical overall RHC and OHC rates at steady-state SCR (Fig. S26 in Supporting Information). Fig. S27 in Supporting Information confirms that the redox model accurately predicts steady-state NO conversion during standard SCR along with NO oxidation rates and NH_3 oxidation rates at different temperatures, feed concentrations and hydrothermal aging conditions. At high temperatures, Cu^{II} reduction during steady-state SCR occurs via gas-phase NH_3 (with and without the direct involvement of NO). Direct oxidation of framework coordinated Cu^{I} ions to ZCuOH sites is followed by consumption of Brønsted NH_3 during subsequent reduction of ZCuOH sites (Eqs. (12)-(13)). Steady-state standard SCR reaction rates increase with temperature up to 250 °C, plateau between 250 °C and 350 °C, and then increase further at high temperatures, qualitatively consistent with expected transition regimes between low and high temperature standard SCR (Fig. S29 in Supporting Information).

In summary, the redox kinetic model developed using a combination of NH_3 TPD and isothermal TRCR protocols successfully predicts transient and steady-state conversions of NO and NH_3 under SCR and oxidation conditions for a wide range of temperatures, feed concentrations and hydrothermal aging states.

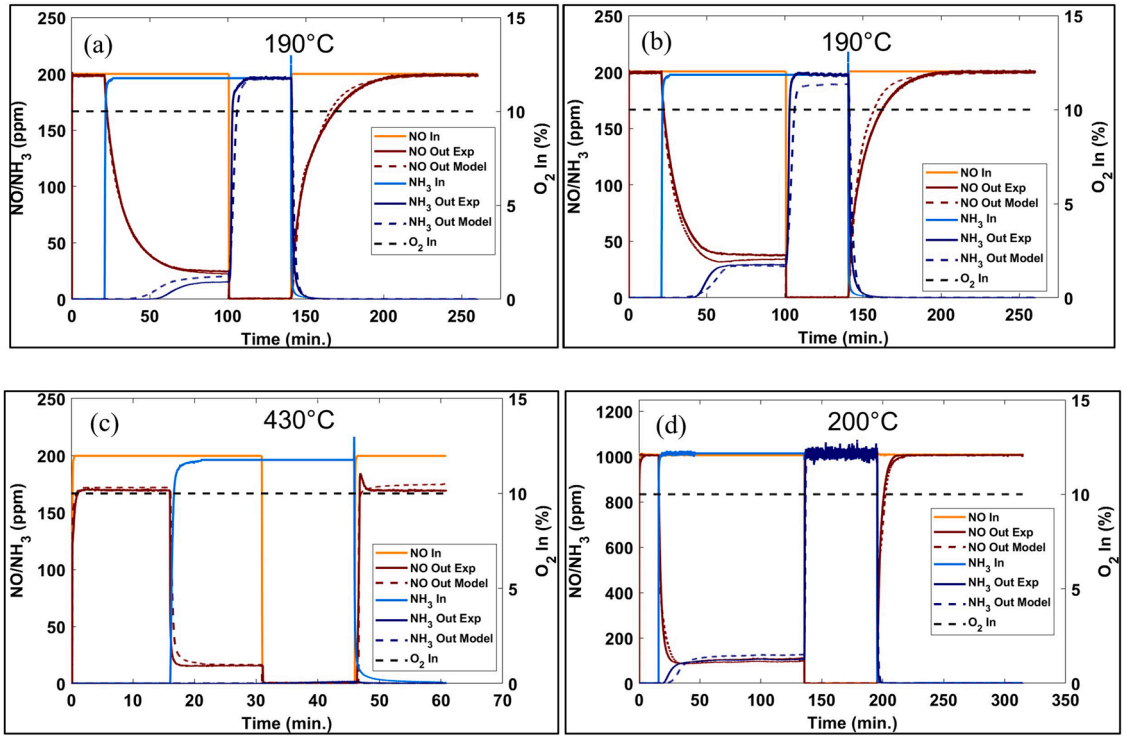

Fig. 13. NO, NH_3 and O_2 concentrations during four-step protocol on (a) degreened (550 °C-4 h) catalyst at 190 °C, (b) hydrothermally aged (650 °C-60 h) catalyst at 190 °C, (c) degreened (550 °C-4 h) catalyst at 430 °C and (d) mild hydrothermally aged (650 °C-5 h) catalyst at 200 °C. GHSV: 60,000 h^{-1}.

4. Discussion

The redox and mobility of active Cu sites has been studied intensively under conditions relevant for low temperature SCR, leading to several mechanistic insights on the low temperature standard SCR reaction catalyzed over Cu-zeolites. However, the dynamics of active Cu sites under high temperature SCR conditions and the corresponding reaction mechanism is not well understood. Spectroscopic experiments elucidating condition dependent Cu speciation can be combined with transient kinetic experiments that alter the oxidation state of Cu in presence of NO, NH_3 and/or O_2 feed gases to inform intrinsic Cu redox rates. This information can be synthesized into redox kinetic models to provide a mechanistic picture of high temperature SCR and associated oxidation reactions.

Fig. 14 demonstrates a schematic of the various redox pathways active in presence of NO, NH_3 or O_2 at low and high temperatures. Reduction of Cu^{II} ions in presence of NO and NH_3 can proceed via four distinct pathways. First, NO can reduce nominally ZCuOH sites (pre-existing and formed from NH_3-assisted hydrolysis of Z_2Cu sites) to form mobile HONO intermediates, which are subsequently consumed by Lewis NH_3, gas-phase NH_3 and/or Brønsted NH_3 [18–21,53]. At low temperatures, RHC involves pairs of NH_3-solvated Cu^{II} sites, and HONO intermediates predominantly consume Lewis NH_3. In absence of Lewis NH_3, RHC occurs over isolated Cu^{II} sites, with the HONO intermediate consuming gas-phase NH_3 and/or Brønsted NH_3 [53,54]. DFT calculations by Liu et al. [55] suggest that the gas-phase NH_3 pathway proceeds via formation of nitrosonium (NO^+) and nitrosamide (NH_2NO) intermediates, has lower energy barriers relative to HONO consumption by Brønsted NH_3, and is inhibited by H_2O. Pairs of HONO intermediates can dehydrate to produce NO and NO_2 [26]. In addition, NO can reduce dimeric Cu^{II} sites to directly form NO_2 [32,35]. Finally, NH_3 can reduce ZCuOH and dimeric Cu^{II} sites to Cu^{I}, forming N_2 in the process [38,44]. NH_3-only RHC proceeds over NH_3-solvated Cu^{II} sites at low temperatures, and over framework coordinated Cu^{II} sites at high temperatures. N_2O formation during NO + NH_3 RHC likely involves reduction of minority NH_3-solvated peroxo dicopper (II) species in presence of NO [59].

Analogous to RHC, low temperature OHC involves pairs of NH_3-solvated Cu sites, proceeding via O_2 activation over Cu^{I} pairs [16,17]. Oxidation of partially solvated and framework coordinated Cu^{I} ions in presence of O_2 also occurs over Cu^{I} pairs. The resulting Cu^{II} dimers can partially hydrate to form pairs of monomeric ZCuOH sites, which in turn can undergo reverse hydrolysis to consume Brønsted acid sites and form monomeric Z_2Cu sites. Unlike RHC, OHC does not consume NH_3 or NO. However, Brønsted NH_3 can be transferred (repartitioned) to Lewis NH_3 during OHC over isolated Cu^{I} sites [38]·H_2O can directly oxidize pairs of Cu^{I} ions at high temperatures [38,46], and may also alter the configuration NH_3-solvated Cu^{II} dimers at low temperatures.

While essential features of the mechanism proposed above are incorporated in the redox model described in this work, it is important to note that this model has several limitations. The explicit quantification and consideration of dimeric Cu^{II} configurations is necessary for chemically consistent descriptions of the NO-only RHC and NH_3-only RHC pathways relevant for NO and NH_3 oxidation reactions respectively. Inclusion of NO oxidation equilibrium constraints is required to describe non-monotonic integral NO_2 formation and NO oxidation as a function of temperature. The simplified NO-only RHC model does not quantitatively predict NO_2 transients during NO oxidation between 250 °C and 400 °C (see Fig. S30 in Supporting Information). The reduction of NH_3-solvated Cu^{II} sites in presence of NH_3 must be considered to predict NH_3 oxidation rates below 350 °C.

OHC reactions representing oxidation of partially solvated and framework coordinated Cu^{I} ions are global in nature. The global OHC model underpredicts integral NO consumption and N_2 formation during oxidation in presence of NO and O_2 at low temperatures. NH_3-release (including Lewis and Brønsted NH_3) concomitant with oxidation of Cu^{I} ions in O_2 is observed but not described at temperatures above 250 °C. Further kinetic and spectroscopic experiments investigating the oxidation of Cu^{I} ions in O_2 are necessary to quantify intrinsic Cu^{I} oxidation rates as a function of temperature and hydrothermal aging. These experiments must also quantify the resulting Cu^{II} speciation relative to the initial Cu^{II} speciation. Additional first-principles calculations of activation barriers and reaction energetics for the redox pathways identified in this work are necessary to guide the development of micro-kinetic models.

The assumptions used in this work are justified by the ability of the kinetic model to accurately reproduce experimental data covering a broad range of SCR and oxidation relevant feed conditions. The overall redox model framework proposed in this work should be more broadly applicable for Cu-Zeolites with varying Cu loading, Si/Al ratios and zeolite types.

5. Conclusions

In this work, we utilized transient response experiments to develop a kinetic model for the redox of active Cu sites under standard SCR and oxidation conditions over a Cu-SSZ-13 catalyst. NO oxidation is a redox

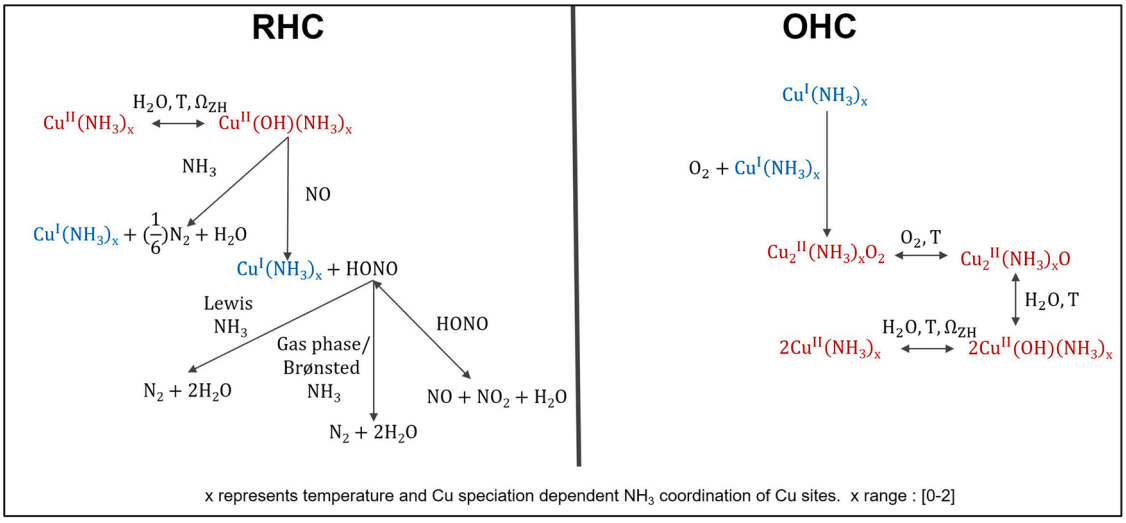

Fig. 14. Schematic representing the redox of Cu sites during standard SCR, NO oxidation and NH_3 oxidation conditions. Oxidation of Cu^{I} by H_2O, nitrite intermediates or NO_2 is not shown in this schematic. x represents temperature and Cu speciation dependent NH_3 coordination of Cu sites. x range: {0−2}.

reaction. Integral NO_2 formation from NO titration experiments is consistent with the production of one NO_2 molecule per two Cu^{II} sites reduced. This indicates that NO_2 forms over two proximal ZCuOH sites and/or mono (μ-oxo) dicopper (II) species (Z_2Cu_2O) during NO oxidation. Decreased NO_2 production upon hydrothermal aging suggests a decreased number density of these Cu configurations on the aged catalyst, quantitatively described by a combination of hydrothermal aging and NO-only RHC kinetic models.

NH_3 oxidation is a redox reaction. Integral N_2 formation from NH_3 titration experiments is consistent with the production of approximately one N_2 molecule per six Cu^{II} sites reduced. Decreased N_2 production upon hydrothermal aging indicates ZCuOH and dimeric Cu^{II} sites catalyze oxidation of NH_3. N_2 formation in presence of NH_3 below 350 °C is associated with the reduction of NH_3-solvated Cu^{II} sites, while N_2 formation above 350 °C is associated with the reduction of framework coordinated Cu^{II} sites. Decrease in high temperature N_2 formation upon hydrothermal aging is predicted by a combination of hydrothermal aging and NH_3-only RHC kinetic models.

NO and NH_3 oxidation reactions share common re-oxidation pathways involving framework coordinated Cu^{I} ions. The oxidation of Cu^{I} pairs in presence of O_2 results in the formation of dimeric Cu^{II} configurations. Monomeric ZCuOH and Z_2Cu sites can be recovered from dimeric Cu^{II} configurations via hydrolysis and reverse hydrolysis reactions that can consume nearby Brønsted acid sites. Brønsted NH_3 can be transferred (repartitioned) to Cu sites during oxidation in presence of O_2. NH_3 and NO do not directly participate in OHC, and no N_2 is produced. However, reduction of Cu^{II} ions occurs during NO + O_2 titration of Cu^{I} ions, resulting in NO consumption and N_2 production. Global OHC kinetic models incorporating these findings successfully predict NO consumption and N_2 production during NO + O_2 titration of Cu^{I} sites as a function of temperature and hydrothermal aging. The resulting redox reaction activation energies are consistent with reported values from kinetic experiments and first-principles calculations.

The redox model is validated with measurements of gas-species during transient response Cu-redox (TRCR) protocols, steady-state SCR conditions and steady-state oxidation conditions. Conversions inflections in N_2 formation observed during standard SCR over pre-reduced and pre-oxidized catalysts are attributed to imbalances in RHC-OHC rates, and quantitatively predicted by the redox model.

The redox reaction mechanism proposed in this work combines recent computational and spectroscopic understanding with kinetic measurements to provide an experimentally validated theoretical framework for standard SCR, NO oxidation and NH_3 oxidation over Cu-SSZ-13. This model also correlates changes in Cu speciation upon hydrothermal aging with the corresponding changes in measured redox rates. The role of H_2O and NO_2 in Cu site redox, along with the influence of sulfur and other chemical contaminants will be reported in the future.

CRediT authorship contribution statement

Rohil Daya: Conceptualization, Methodology, Formal analysis, Investigation, Data curation, Writing – original draft, Visualization. **Dhruba J. Deka**: Methodology, Validation, Formal analysis, Investigation, Data curation, Writing – review & editing. **Anshuman Goswami**: Formal analysis, Data curation, Writing – review & editing. **Unmesh Menon**: Methodology, Investigation, Data curation, Writing – review & editing. **Dylan Trandal**: Methodology, Investigation, Data curation, Writing – review & editing. **William P. Partridge**: Conceptualization, Supervision, Writing – review & editing. **Saurabh Y. Joshi**: Conceptualization, Supervision, Writing – review & editing.

Declaration of Competing Interest

The authors declare the following financial interests/personal relationships which may be considered as potential competing interests: William P. Partridge reports financial support was provided by US Department of Energy.

Data availability

Data will be made available on request.

Acknowledgements

This research was supported in part by the DOE Office of Energy Efficiency and Renewable Energy (EERE) Vehicle Technologies Office (VTO) and used resources at the National Transportation Research Center, a DOE-EERE User Facility at Oak Ridge National Laboratory (ORNL). We thank Neal Currier, Michael Cunningham, Krishna Kamasamudram and Aleksey Yezerets from Cummins Inc. for their valuable support and promotion of the ORNL-Cummins Catalyst CRADA (cooperative research and development agreement) partnership (No. 97-0489) within which a portion of this work was performed, and their SCR-catalyst insights. We thank Josh Pihl, group leader of the ORNL Applied Catalysis and Emissions Research Group, for his critical review and suggestions regarding catalysis methods and experiments, and help with experimental system automation. We thank DOE VTO Program & Technology Managers: Gurpeet Singh, Siddiq Khan, and Ken Howden for supporting the CRADA project.

Supporting Information

Supporting Information includes additional model validation with measured transient and integral N_2 over the ten-step TRCR protocol. Turnover rates, Cu^{II} fraction and NH_3 storage predictions during this protocol from 200 °C to 450 °C are also provided. Redox model validation with transient and steady-state NO/NH_3 consumption during TRCR protocols and the four-step protocol is shown, along with corresponding model predictions of mean surface coverage and overall reaction rates as a function of time and temperature.

Appendix A. Supporting information

Supplementary data associated with this article can be found in the online version at doi:10.1016/j.apcatb.2023.122524.

References

[1] F. Gao, C.H. Peden, Recent progress in atomic-level understanding of Cu/SSZ-13 selective catalytic reduction catalysts, Catalysts 8 (4) (2018) 140.
[2] C. Paolucci, J.R. Di Iorio, F.H. Ribeiro, R. Gounder, W.F. Schneider, Catalysis science of NOx selective catalytic reduction with ammonia over Cu-SSZ-13 and Cu-SAPO-34, in: Advances in Catalysis, vol. 59, Academic Press, 2016, pp. 1–107.
[3] C. Paolucci, A.A. Parekh, I. Khurana, J.R. Di Iorio, H. Li, J.D. Albarracin Caballero, W.F. Schneider, Catalysis in a cage: condition-dependent speciation and dynamics of exchanged Cu cations in SSZ-13 zeolites, J. Am. Chem. Soc. 138 (18) (2016) 6028–6048.
[4] J.R. Di Iorio, S.A. Bates, A.A. Verma, W.N. Delgass, F.H. Ribeiro, J.T. Miller, R. Gounder, The dynamic nature of Brønsted acid sites in Cu–zeolites during NOx selective catalytic reduction: quantification by gas-phase ammonia titration, Top. Catal. 58 (7) (2015) 424–434.
[5] A. Martini, E. Borfecchia, K.A. Lomachenko, I.A. Pankin, C. Negri, G. Berlier, C. Lamberti, Composition-driven Cu-speciation and reducibility in Cu-CHA zeolite catalysts: a multivariate XAS/FTIR approach to complexity, Chem. Sci. 8 (10) (2017) 6836–6851.
[6] R. Villamaina, S. Liu, I. Nova, E. Tronconi, M.P. Ruggeri, J. Collier, D. Thompsett, Speciation of Cu cations in Cu-CHA catalysts for NH3-SCR: effects of SiO2/AlO3 ratio and Cu-loading investigated by transient response methods, ACS Catal. 9 (10) (2019) 8916–8927.
[7] Y. Zhang, Y. Wu, Y. Peng, J. Li, E.D. Walter, Y. Chen, F. Gao, Quantitative Cu counting methodologies for Cu/SSZ-13 selective catalytic reduction catalysts by electron paramagnetic resonance spectroscopy, J. Phys. Chem. C 124 (51) (2020) 28061–28073.
[8] J.R. Di Iorio, S. Li, C.B. Jones, C.T. Nimlos, Y. Wang, E. Kunkes, R. Gounder, Cooperative and competitive occlusion of organic and inorganic structure-directing agents within chabazite zeolites influences their aluminum arrangement, J. Am. Chem. Soc. 142 (10) (2020) 4807–4819.
[9] J.H. Kwak, H. Zhu, J.H. Lee, C.H. Peden, J. Szanyi, Two different cationic positions in Cu-SSZ-13? Chem. Commun. 48 (39) (2012) 4758–4760.

[10] A. Godiksen, F.N. Stappen, P.N. Vennestrøm, F. Giordanino, S.B. Rasmussen, L. F. Lundegaard, S. Mossin, Coordination environment of copper sites in Cu-CHA zeolite investigated by electron paramagnetic resonance, J. Phys. Chem. C 118 (40) (2014) 23126–23138.
[11] B. Ipek, M.J. Wulfers, H. Kim, F. Goltl, I. Hermans, J.P. Smith, R.F. Lobo, Formation of [Cu2O2] 2+ and [Cu2O] 2+ toward C–H bond activation in Cu-SSZ-13 and Cu-SSZ-39, ACS Catal. 7 (7) (2017) 4291–4303.
[12] H. Li, C. Paolucci, I. Khurana, L.N. Wilcox, F. Göltl, J.D. Albarracin-Caballero, W. F. Schneider, Consequences of exchange-site heterogeneity and dynamics on the UV–visible spectrum of Cu-exchanged SSZ-13, Chem. Sci. 10 (8) (2019) 2373–2384.
[13] C. Negri, M. Signorile, N.G. Porcaro, E. Borfecchia, G. Berlier, T.V. Janssens, S. Bordiga, Dynamic CuII/CuI speciation in Cu-CHA catalysts by in situ Diffuse Reflectance UV–vis–NIR spectroscopy, Appl. Catal. A Gen. 578 (2019) 1–9.
[14] U. Engedahl, H. Grönbeck, A. Hellman, First-principles study of oxidation state and coordination of Cu-dimers in Cu-SSZ-13 during methane-to-methanol reaction conditions, J. Phys. Chem. C 123 (43) (2019) 26145–26150.
[15] F. Goltl, S. Bhandari, M. Mavrikakis, Thermodynamics perspective on the stepwise conversion of methane to methanol over Cu-exchanged SSZ-13, ACS Catal. 11 (13) (2021) 7719–7734.
[16] C. Paolucci, I. Khurana, A.A. Parekh, S. Li, A.J. Shih, H. Li, R. Gounder, Dynamic multinuclear sites formed by mobilized copper ions in NO x selective catalytic reduction, Science 357 (6354) (2017) 898–903.
[17] F. Gao, D. Mei, Y. Wang, J. Szanyi, C.H. Peden, Selective catalytic reduction over Cu/SSZ-13: linking homo-and heterogeneous catalysis, J. Am. Chem. Soc. 139 (13) (2017) 4935–4942.
[18] L. Chen, T.V. Janssens, P.N. Vennestrøm, J. Jansson, M. Skoglundh, H. Gronbeck, A complete multisite reaction mechanism for low-temperature NH3-SCR over Cu-CHA, ACS Catal. 10 (10) (2020) 5646–5656.
[19] W. Hu, T. Selleri, F. Gramigni, E. Fenes, K.R. Rout, S. Liu, E. Tronconi, On the redox mechanism of low-temperature NH3–SCR over Cu-CHA: a combined experimental and theoretical study of the reduction half cycle, Angew. Chem. Int. Ed. 60 (13) (2021) 7197–7204.
[20] W. Hu, U. Iacobone, F. Gramigni, Y. Zhang, X. Wang, S. Liu, E. Tronconi, Unraveling the hydrolysis of Z2Cu2+ to ZCu2+ (OH)− and its consequences for the low-temperature selective catalytic reduction of NO on Cu-CHA catalysts, ACS Catal. 11 (18) (2021) 11616–11625.
[21] R. Daya, D. Trandal, U. Menon, D.J. Deka, W.P. Partridge, S.Y. Joshi, Kinetic model for the reduction of CuII sites by NO+ NH3 and reoxidation of NH3-solvated CuI sites by O2 and NO in Cu-SSZ-13, ACS Catal. 12 (2022) 6418–6433.
[22] Y. Wu, Y. Ma, Y. Wang, K.G. Rappé, N.M. Washton, Y. Wang, F. Gao, Rate controlling in low-temperature standard NH3-SCR: implications from operando EPR spectroscopy and reaction kinetics, J. Am. Chem. Soc. (2022).
[23] C. Paolucci, J.R. Di Iorio, W.F. Schneider, R. Gounder, Solvation and mobilization of copper active sites in zeolites by ammonia: consequences for the catalytic reduction of nitrogen oxides, Acc. Chem. Res. 53 (9) (2020) 1881–1892.
[24] R. Daya, D. Trandal, R.K. Dadi, H. Li, S.Y. Joshi, J. Luo, A. Yezerets, Kinetics and thermodynamics of ammonia solvation on Z2Cu, ZCuOH and ZCu sites in Cu-SSZ-13–Implications for hydrothermal aging, Appl. Catal. B Environ. 297 (2021), 120444.
[25] W. Hu, F. Gramigni, N.D. Nasello, N. Usberti, U. Iacobone, S. Liu, E. Tronconi, Dynamic binuclear CuII sites in the reduction half-cycle of low-temperature NH3–SCR over Cu-CHA catalysts, ACS Catal. 12 (9) (2022) 5263–5274.
[26] N. Usberti, F. Gramigni, N.D. Nasello, U. Iacobone, T. Selleri, W. Hu, E. Tronconi, An experimental and modelling study of the reactivity of adsorbed NH3 in the low temperature NH3-SCR reduction half-cycle over a Cu-CHA catalyst, Appl. Catal. B Environ. 279 (2020), 119397.
[27] D.J. Deka, R. Daya, A. Ladshaw, S.Y. Joshi, W.P. Partridge, A transient-response methodology based on experiments and modeling for cu-redox half-cycle kinetic analysis on a Cu-SSZ-13 SCR catalyst, Chem. Eng. J. (2021), 134219.
[28] A.R. Fahami, T. Günter, D.E. Doronkin, M. Casapu, D. Zengel, T.H. Vuong, J. D. Grunwaldt, The dynamic nature of Cu sites in Cu-SSZ-13 and the origin of the seagull NO x conversion profile during NH 3-SCR, React. Chem. Eng. 4 (6) (2019) 1000–1018.
[29] T.V. Janssens, H. Falsig, L.F. Lundegaard, P.N. Vennestrøm, S.B. Rasmussen, P. G. Moses, P. Beato, A consistent reaction scheme for the selective catalytic reduction of nitrogen oxides with ammonia, ACS Catal. 5 (5) (2015) 2832–2845.
[30] Y. Zhang, Y. Peng, K. Li, S. Liu, J. Chen, J. Li, C.H. Peden, Using transient FTIR spectroscopy to probe active sites and reaction intermediates for selective catalytic reduction of NO on Cu/SSZ-13 catalysts, ACS Catal. 9 (7) (2019) 6137–6145.
[31] C. Paolucci, A.A. Verma, S.A. Bates, V.F. Kispersky, J.T. Miller, R. Gounder, W. F. Schneider, Isolation of the copper redox steps in the standard selective catalytic reduction on Cu-SSZ-13, Angew. Chem. Int. Ed. 53 (44) (2014) 11828–11833.
[32] A.A. Verma, S.A. Bates, T. Anggara, C. Paolucci, A.A. Parekh, K. Kamasamudram, F.H. Ribeiro, NO oxidation: a probe reaction on Cu-SSZ-13, J. Catal. 312 (2014) 179–190.
[33] F. Gao, E.D. Walter, M. Kollar, Y. Wang, J. Szanyi, C.H. Peden, Understanding ammonia selective catalytic reduction kinetics over Cu/SSZ-13 from motion of the Cu ions, J. Catal. 319 (2014) 1–14.
[34] M.P. Ruggeri, I. Nova, E. Tronconi, J.A. Pihl, T.J. Toops, W.P. Partridge, In-situ DRIFTS measurements for the mechanistic study of NO oxidation over a commercial Cu-CHA catalyst, Appl. Catal. B Environ. 166 (2015) 181–192.
[35] I. Khurana, J.D. Albarracin-Caballero, A.J. Shih, Identification and quantification of multinuclear Cu active sites derived from monomeric Cu moieties for dry NO oxidation over Cu-SSZ-13, J. Catal. (2022).
[36] F. Giordanino, E. Borfecchia, K.A. Lomachenko, A. Lazzarini, G. Agostini, E. Gallo, C. Lamberti, Interaction of NH3 with Cu-SSZ-13 catalyst: a complementary FTIR, XANES, and XES study, J. Phys. Chem. Lett. 5 (9) (2014) 1552–1559.
[37] T. Günter, H.W. Carvalho, D.E. Doronkin, T. Sheppard, P. Glatzel, A.J. Atkins, J. D. Grunwaldt, Structural snapshots of the SCR reaction mechanism on Cu-SSZ-13, Chem. Commun. 51 (44) (2015) 9227–9230.
[38] D.J. Deka, R. Daya, S.Y. Joshi, W.P. Partridge, On the various Cu-redox pathways and O2-mediated Bronsted-to-Lewis adsorbed-NH3 redistribution under SCR half-cycle conditions, Appl. Catal. A Gen. (2022), 118656.
[39] Y. Zhang, J. Zhang, H. Wang, W. Yang, C. Wang, Y. Peng, F. Gao, Selective catalytic reduction of NO x with NH3 over Cu/SSZ-13: elucidating dynamics of Cu active sites with in situ UV–Vis spectroscopy and DFT calculations, J. Phys. Chem. C (2022).
[40] F. Gao, N.M. Washton, Y. Wang, M. Kollár, J. Szanyi, C.H. Peden, Effects of Si/Al ratio on Cu/SSZ-13 NH3-SCR catalysts: implications for the active Cu species and the roles of Brønsted acidity, J. Catal. 331 (2015) 25–38.
[41] M. Moreno-González, B. Hueso, M. Boronat, T. Blasco, A. Corma, Ammonia-containing species formed in Cu-chabazite as per in situ EPR, solid-state NMR, and DFT calculations, J. Phys. Chem. Lett. 6 (6) (2015) 1011–1017.
[42] Y. Ma, X. Wu, J. Ding, L. Liu, B. Jin, E.D. Walter, D. Weng, Quasi-operando quantification of Cu (ii) ions in Cu-SSZ-13 catalyst by an NH 3 temperature-programmed reduction method, Chem. Commun. 57 (15) (2021) 1891–1894.
[43] R. Villamaina, F. Gramigni, U. Iacobone, S. Liu, I. Nova, E. Tronconi, D. Thompsett, The H2O effect on Cu speciation in Cu-CHA-Catalysts for NH3-SCR probed by NH3 titration, Catalysts 11 (7) (2021) 759.
[44] L.N. Wilcox, S.H. Krishna, C.B. Jones, R. Gounder, Mechanistic studies of NH 3-assisted reduction of mononuclear Cu (ii) cation sites in Cu-CHA zeolites, Catal. Sci. Technol. 11 (24) (2021) 7932–7942.
[45] J. Luo, H. An, K. Kamasamudram, N. Currier, A. Yezerets, T. Watkins, L. Allard, Impact of accelerated hydrothermal aging on structure and performance of Cu-SSZ-13 SCR catalysts, SAE Int. J. Engines 8 (3) (2015) 1181–1186.
[46] V.L. Sushkevich, D. Palagin, M. Ranocchiari, J.A. Van Bokhoven, Selective anaerobic oxidation of methane enables direct synthesis of methanol, Science 356 (6337) (2017) 523–527.
[47] U. Engedahl, H. Grönbeck, A. Hellman, First-principles study of oxidation state and coordination of cu-dimers in Cu-SSZ-13 during methane-to-methanol reaction conditions, J. Phys. Chem. C 123 (43) (2019) 26145–26150.
[48] K.T. Dinh, M.M. Sullivan, K. Narsimhan, P. Serna, R.J. Meyer, M. Dincă, Y. Román-Leshkov, Continuous partial oxidation of methane to methanol catalyzed by diffusion-paired copper dimers in copper-exchanged zeolites, J. Am. Chem. Soc. 141 (29) (2019) 11641–11650.
[49] D.T. Bregante, L.N. Wilcox, C. Liu, C. Paolucci, R. Gounder, D.W. Flaherty, Dioxygen activation kinetics over distinct cu site types in cu-chabazite zeolites, ACS Catal. 11 (19) (2021) 11873–11884.
[50] J. Luo, F. Gao, K. Kamasamudram, N. Currier, C.H. Peden, A. Yezerets, New insights into Cu/SSZ-13 SCR catalyst acidity. Part I: nature of acidic sites probed by NH3 titration, J. Catal. 348 (2017) 291–299.
[51] K. Kamasamudram, N.W. Currier, X. Chen, A. Yezerets, Overview of the practically important behaviors of zeolite-based urea-SCR catalysts, using compact experimental protocol, Catal. Today 151 (3–4) (2010) 212–222.
[52] C. Liu, H. Kubota, T. Toyao, Z. Maeno, K.I. Shimizu, Mechanistic insights into the oxidation of copper (i) species during NH 3-SCR over Cu-CHA zeolites: a DFT study, Catal. Sci. Technol. 10 (11) (2020) 3586–3593.
[53] R. Daya, C.J. Keturakis, D. Trandal, A. Kumar, S.Y. Joshi, A. Yezerets, Alternate pathway for standard SCR on Cu-zeolites with gas-phase ammonia, React. Chem. Eng. 6 (6) (2021) 1042–1052.
[54] H. Kubota, T. Toyao, Z. Maeno, Y. Inomata, T. Murayama, N. Nakazawa, K. I. Shimizu, Analogous mechanistic features of NH3-SCR over vanadium oxide and copper zeolite catalysts, ACS Catal. 11 (17) (2021) 11180–11192.
[55] C. Liu, S. Yasumura, T. Toyao, Z. Maeno, K.I. Shimizu, Mechanism of standard NH3–SCR over Cu-CHA via NO+ and HONO intermediates, J. Phys. Chem. C 126 (28) (2022) 11594–11601.
[56] A. Marberger, A.W. Petrov, P. Steiger, M. Elsener, O. Kröcher, M. Nachtegaal, D. Ferri, Time-resolved copper speciation during selective catalytic reduction of NO on Cu-SSZ-13, Nat. Catal. 1 (3) (2018) 221–227.
[57] S.H. Krishna, C.B. Jones, R. Gounder, Temperature dependence of Cu (I) oxidation and Cu (II) reduction kinetics in the selective catalytic reduction of NOx with NH3 on Cu-chabazite zeolites, J. Catal. 404 (2021) 873–882.
[58] W.P. Partridge, S.Y. Joshi, J.A. Pihl, N.W. Currier, New operando method for quantifying the relative half-cycle rates of the NO SCR redox cycle over Cu-exchanged zeolites, Appl. Catal. B Environ. 236 (2018) 195–204.
[59] Y. Xi, N.A. Ottinger, C.J. Keturakis, Z.G. Liu, Dynamics of low temperature N2O formation under SCR reaction conditions over a Cu-SSZ-13 catalyst, Appl. Catal. B Environ. 294 (2021), 120245.